Astronomy
&
Astrophysics

A Chandra and Spitzer census of the young star cluster in the reflection nebula NGC 7129[⋆]

B. Stelzer[1] and A. Scholz[2]

[1] INAF – Osservatorio Astronomico di Palermo, Piazza del Parlamento 1, 90134 Palermo, Italy
e-mail: [B.Stelzer;stelzer]@astropa.unipa.it
[2] SUPA, School of Physics & Astronomy, University of St. Andrews, North Haugh, St. Andrews KY 16 9SS, UK

ABSTRACT

Context. The reflection nebula NGC 7129 has long been known to be a site of recent star formation as shown, e.g., by the presence of deeply embedded protostars and HH objects. However, studies of the stellar population produced in the star formation process have remained rudimentary. A major step forward has been made with recent Spitzer imaging of the region.
Aims. This study represents the next step towards a systematic assessment of the pre-main sequence population in NGC 7129. Completeness of the pre-main sequence sample is necessary for studying key features that allow the star-forming process to be understood, such as disk evolution, dynamical evolution, and mass function. At a presumed age of ~3 Myr, NGC 7129 is in the critical range where disks around young stars disappear.
Methods. We make use of X-ray and IR imaging observations to identify the pre-main sequence stars in NGC 7129. We define a sample of young stellar objects based on color–color diagrams composed from IR photometry between 1.6 and 8 μm, from 2 MASS and Spitzer, and based on X-ray detected sources from a Chandra observation.
Results. This sample is composed of 26 Class II and 25 Class III candidates. It has been selected from infrared sources in the Chandra field (287 objects with photometry in all four Spitzer/IRAC bands, 811 objects with near-IR photometry) and the 59 X-ray sources detected with Chandra. The sample is estimated to be complete down to ~0.5 $M_\odot$. The most restricted and least biased subsample of pre-main sequence stars is composed of lightly absorbed ($A_V < 5$ mag) stars in the cluster core. This sample comprises 7 Class II and 14 Class III sources and has a disk fraction of $33^{+24}_{-19}\%$ and a median X-ray luminosity of log L_x [erg/s] = 30.3.
Conclusions. Despite the various uncertainties related to the sample selection, absorption, mass distribution, distance, and, consequently in the computation of disk fraction and X-ray luminosities, the data yield consistent results. In particular, we confirm the age of ~3 Myr for the NGC 7129 cluster. The derived disk fraction is similar to that of σ Orionis, smaller than for Cha I (~2 Myr), and larger than for Upper Sco (5 Myr). The X-ray luminosity function is similar to that of NGC 2264 (2 Myr) but fainter than for the Orion Nebula Cluster (1 Myr). The pre-main sequence census should be further refined and extended with optical photometric and spectroscopic searches for cluster members.

Key words. X-rays: stars – infrared: stars – stars: pre-main sequence – stars: formation

1. Introduction

Young stars undergo various phases on their way to the main-sequence. Their different evolutionary stages are recognized by specific observational features, such as excess emission over the expectation for a stellar photosphere that arises from circumstellar matter. Initially, Young Stellar Objects (YSOs) are embedded in envelopes of cold and dusty material that emit prominently at infrared (IR) and sub-millimeter wavelengths. The youngest, protostellar phases are termed Class 0 and Class I in a classification scheme based on the spectral energy distribution (SED) (Lada 1987). As their evolution proceeds, disk accretion and re-processing of stellar light in the disk become the identifying feature and the YSO is of Class II. Finally, when all circumstellar matter has dispersed or accreted onto the star a Class III object is left that is unconspicuous at IR bands as its SED is purely photospheric.

Low sensitivity of mid-IR detectors have long hampered systematic searches for the signatures of circumstellar matter revealing young stars in their accretion and/or embedded phases.

The launch of *Spitzer* has dramatically increased the census of YSOs in various star-forming regions (see e.g. Evans et al. 2009, and references therein). However, as suggested above, IR observations have no potential for distinguishing young stars after the disk has dispersed from evolved stars. Therefore, a YSO census based on IR data alone is highly biased and other techniques are needed to reveal the Class III population. Diskless stars can, indeed, be identified on the basis of their strong X-ray emission, a prevalent characteristic for the whole pre-main sequence (pre-MS) evolution. The X-ray and IR observations thus provide complementary tools for identifying the complete pre-MS population. Knowing all members of a given star-forming region is essential for understanding fundamental problems, such as disk evolution, dynamical evolution, and the initial mass function.

We present here a *Chandra* X-ray and *Spitzer* IR census of the star cluster in NGC 7129. According to Racine (1968), the NGC 7129 reflection nebula in Cepheus is located at a distance of ~1 kpc. Shevchenko & Yakubov (1989) published a value of 1260 ± 50 pc. Both distance estimates are based on optical photometry of few stars and ought to be considered quite uncertain. NGC 7129 is dominated by the young B-type stars BD + 65 1637 (SVS 7) and BD +65 1638 (SVS 8) in a

---

cavity surrounded by dense molecular ridges that form the interface with the molecular cloud (Miskolczi et al. 2001). A third Herbig Be star, LkHα 234 (SVS 12), is located on the eastern end of the ridge. SVS 12 was presumably formed in the ridge following compression of material (Bechis et al. 1978). Further signs of very recent star formation in NGC 7129 are deeply embedded protostars identified in IR images (Weintraub et al. 1994; Cabrit et al. 1997), and a large outflow initially thought to originate in SVS 12, but later assigned to an embedded pre-MS object IRS 6 located 3″ of the Herbig star (Cabrit et al. 1997; Fuente et al. 2001). The region also contains the probably youngest intermediate-mass object known at present, the Class 0 star FIRS-2 (Eiroa et al. 1998; Fuente et al. 2005). Several Herbig-Haro outflows (Hartigan & Lada 1985; Strom et al. 1986; Miranda et al. 1993) and a cluster of low-mass pre-MS stars are associated with NGC 7129. The most recent census of optical emission line stars counts 22 objects (Magakian et al. 2004).

Spitzer imaging observations for NGC 7129 have been reported by Gutermuth et al. (2004) and Muzerolle et al. (2004). With a combination of IR photometry from ground-based observations, 2 MASS and IRAC a total of 84 objects with circumstellar disks could be identified, half of them in the 0.5 pc wide cluster core. The longer wavelength images obtained with MIPS are dominated in the central region of NGC 7129 by nebular emission. Therefore, MIPS could detect YSOs only in the outer parts of the reflection nebula. The discovery of over 10 protostars in the outskirts of the cluster led Muzerolle et al. (2004) to suggest that the area of active star formation in NGC 7129 extends over a large area of ∼3 pc.

NGC 7129 has now been studied at virtually all wavelengths from the submillimeter (Font et al. 2001) to optical bands but a systematic investigation of X-ray emission from the pre-MS population is absent from the literature. We close this important gap with a *Chandra* observation of NGC 7129 that we combine with *Spitzer* photometry and data at other wavelengths from the literature for the few previously known cluster members. This new assessment of the cluster population is a solid basis for future optical photometric and spectroscopic observations with the aim of confirming the new members. Section 2 describes the X-ray data analysis. We give a brief description of the *Spitzer* photometry provided to us by Gutermuth (Sect. 3) and of the optical catalog of NGC 7129 (Sect. 4). We present our selection criteria for YSOs and the resulting census of NGC 7129 members in Sect. 5. In Sect. 6 the results are presented. We discuss selected SEDs, derive the disk fraction and the X-ray luminosity function for the pre-MS cluster, and add a note on the X-ray emission from protostars. A summary and conclusions are given in Sect. 7.

2. *Chandra* data analysis

A 22 ks long *Chandra* observation targeting the Herbig star SVS 12 was carried out on Mar 11, 2006 (start of observation UT $14^h29^m18^s$). The observation was obtained within a survey for X-ray emission from Herbig stars, and the data for the three B-type stars in the field-of-view has been presented by Stelzer et al. (2009). The prime instrument for this observation was ACIS-S3 because of the higher sensitivity at low energies of the ACIS spectroscopic array with respect to the imaging array. ACIS-S2 and all four ACIS-I chips were turned on as well.

SVS 12 lies at the heart of the NGC 7129 reflection nebula, giving serendipitously access to study for the first time the X-ray emission from the associated young star cluster. The cluster core was estimated by Gutermuth et al. (2004) from K_S band star counts to comprise a 0.5 pc radius, corresponding to less than 2′ at the distance of 1 kpc. Therefore, most X-ray sources are expected to be located on a single ACIS chip. We analyzed only data from ACIS-S3 and ACIS-S2 that overlap (partially) with the *Spitzer* survey. Figure 1 shows the Chandra ACIS-S2 and ACIS-S3 image with the Spitzer/IRAC field overlaid. The cluster core of ∼1.7′ radius (Gutermuth et al. 2004) is marked as red circle.

The data analysis was performed with the CIAO software package[1] version 4.0. We started our analysis with the level 1 events file provided by the *Chandra* X-ray Center (CXC). In the process of converting the level 1 events file to a level 2 events file for each of the observations, we performed the following steps: We removed the pixel randomization that is automatically applied by the CXC pipeline in order to optimize the spatial resolution. We filtered the events file for event grades (retaining the standard grades 0, 2, 3, 4, and 6), and applied the standard good time interval file. Events flagged as cosmic rays were not removed in our analysis. In principle, such events can lead to detecting spurious sources. However, if identified on the position of a bright X-ray source, the flag is often erroneous (as a result of the event pattern used for identifying cosmic rays).

Source detection was carried out in the 0.3–10 keV band for the ACIS-S3 and ACIS-S2 chips with the WAVDETECT algorithm (Freeman et al. 2002) using an image with spatial resolution of 0.5″/pixel and a congruent, monochromatic exposure map for 1.5 keV. The WAVDETECT algorithm correlates the data with a Mexican hat function to search for deviations from the background. This method is well suited for separating closely spaced point sources. We used wavelet scales between 1 and 8 in steps of $\sqrt{2}$. The detection significance was set to 10^{-6} to avoid spurious detections.

We cleaned the resulting source list on the basis of the individual signal-to-noise ratio (S/N) of each detection. First, the point-spread-function (PSF) was computed for each X-ray position. A circular source photon extraction region was defined as the area that contains 90% of the PSF. The background was extracted individually from a squared region centered on and several times larger than the source extraction area. If detected X-ray sources were in the selected background area a circular area around them was eliminated from the background region. The S/N was computed from the counts summed in the source and background areas, respectively, after applying the appropriate area scaling factor to the background counts. In general, the background is negligibly low. We removed all objects with $S/N < 3$ as likely to be spurious from the WAVDETECT X-ray source list. In Table 2 we provide the final list of 59 X-ray sources.

There are only 5 X-ray sources with more than 100 counts in the 0.3–10 keV band (sources NGC 7129-S3-X2,..-X12,..-X13,...-X23, and NGC 7129-S2-X9) such that a detailed spectral analysis is not feasible for most objects. We extracted and analyzed the X-ray spectra for the five brightest sources mentioned above. An individual response matrix and auxiliary response were extracted for each of them using standard CIAO tools. Each spectrum was binned to a minimum of 5 or more counts per bin depending on the photon statistics. As the background of ACIS is very low (<1 count in the source extraction area), it can be neglected. We fitted each spectrum in the XSPEC 12.4.0 environment with a one-temperature thermal model spectrum (Raymond & Smith 1977) subject to photo-absorption (WABS * APEC).
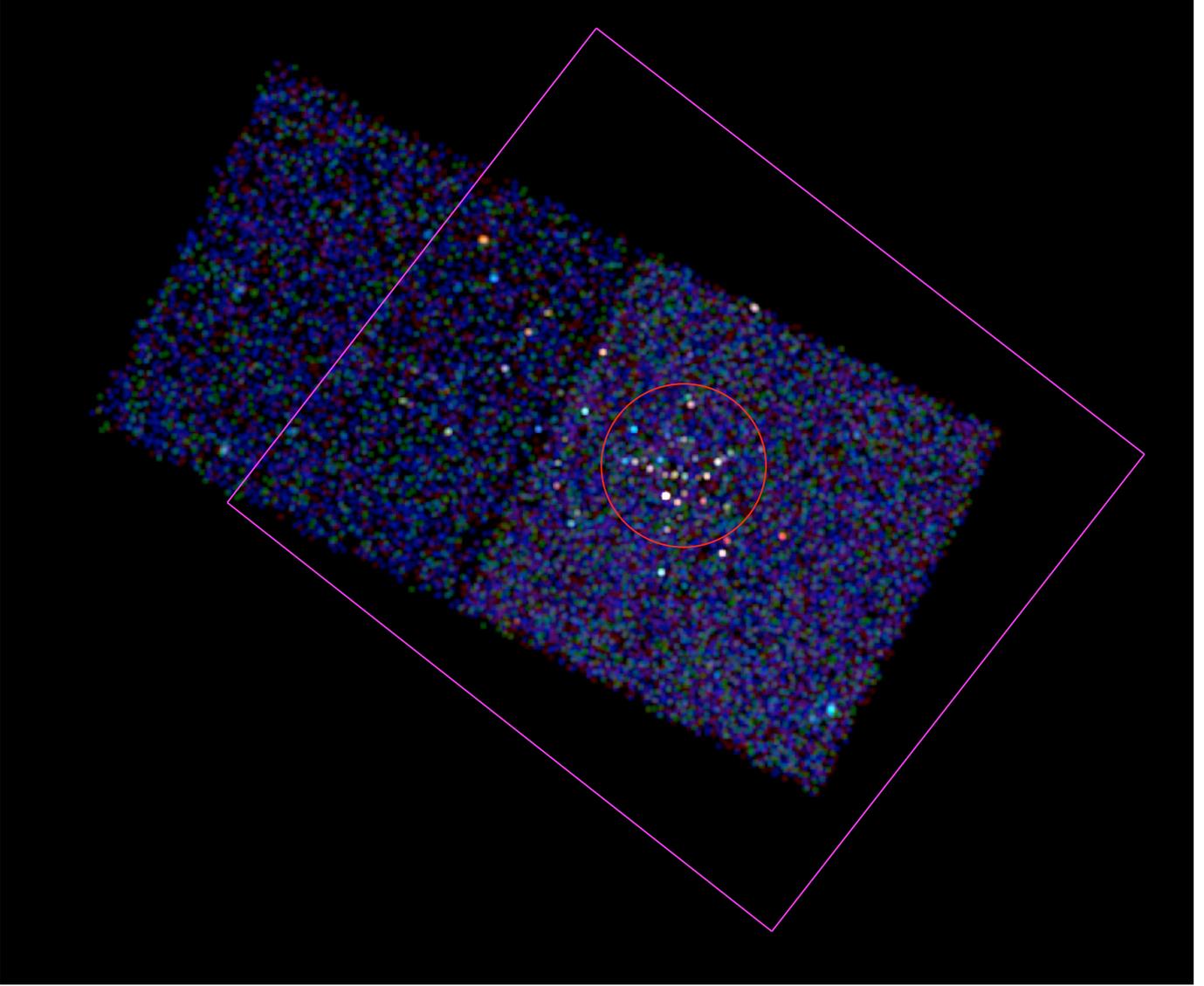
Fig. 1. *Chandra* false–color image of NGC 7129 (data shown is from ACIS-S2 and ACIS-S3 chips). The large rectangle is the IRAC field-of-view (circa $12.6' \times 14.5'$), and the circle shows the $\sim 1.7'$ cluster core as defined by Gutermuth et al. (2004). Evidently, the bulk of X-ray sources is concentrated in the area of the cluster core.

More complex spectral models are not considered because of the low statistics of these data. Figure 2 shows the data with the best fit spectral models and χ^2 residuals. For NGC 7129-S3-X12 and NGC 7129-S3-X13, which are partially overlapping, we used the photon extraction regions defined by Stelzer et al. (2009). All five spectra are compatible with $\log N_H \,[\mathrm{cm}^{-2}] < 22$ and kT in the range of $1...2\,\mathrm{keV}$.

In cases of low photon statistics it is common practice to examine X-ray hardness ratios. We define three energy bands: soft ($S = 0.2-1.7\,\mathrm{keV}$), medium ($M = 1.7-2.8\,\mathrm{keV}$), and hard ($H = 2.8-8.0\,\mathrm{keV}$) from which we construct two colors following Albacete Colombo et al. (2007), S/M and M/H. Figure 3 shows the hardness ratio diagram where a grid calculated from a one-temperature thermal model with photo-absorption is overlaid. The majority of X-ray sources are compatible with a temperature of $1...2\,\mathrm{keV}$ and moderate ($\leq 10^{22}\,\mathrm{cm}^{-2}$) absorption. For three of the five sources discussed in the previous paragraph, the N_H and kT derived from Fig. 3 agree within the 90 % confidence level with the values obtained from the spectral fitting. For NGC 7129-S3-X12 and NGC 7129-S3-X13, the XSPEC fits

yield a cooler and less absorbed spectrum than the hardness ratios. These are the two stars with the best photon statistics, so a $1 - T$ approach may not be appropriate.

Column densities and temperatures inferred from X-ray hardness ratios can in principle be used to derive X-ray luminosities of individual stars when the statistics are too poor for detailed spectral analysis. However, as seen above in the comparison to the spectral results for the brightest stars, even the use of hardness ratios may be associated with large uncertainties. Furthermore, not all data points lie in the region covered by physically reasonable models (see Fig. 3). For calculating the X-ray luminosities of objects outside the grid, we used the median temperature and absorbing column of the sample with >20 net source counts, while for all objects on the grid we used their individual N_H and kT estimates. Moreover, we anticipate in Fig. 3 a trend toward higher absorption for Class II with respect to Class III sources. (The YSO classification scheme is described in Sect. 5.) Therefore, we computed separate medians for these two YSO groups. We find a median of $N_{H,C\,II} = 8.8 \times 10^{21}\,\mathrm{cm}^{-2}$ for Class II and of $N_{H,C\,III} = 2.1 \times 10^{21}\,\mathrm{cm}^{-2}$ for Class III. These
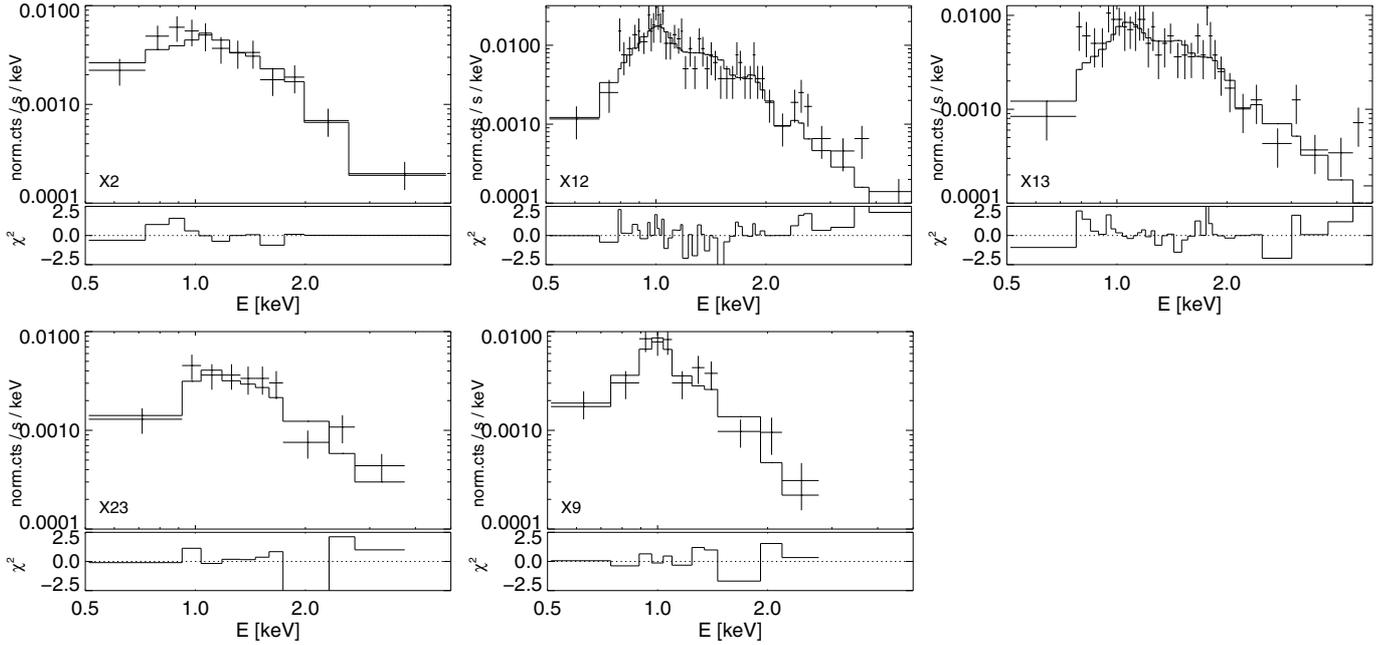
Fig. 2. X-ray spectra for the five brightest sources in NGC 7129, best-fitting absorbed one-temperature model and χ^2 residuals.
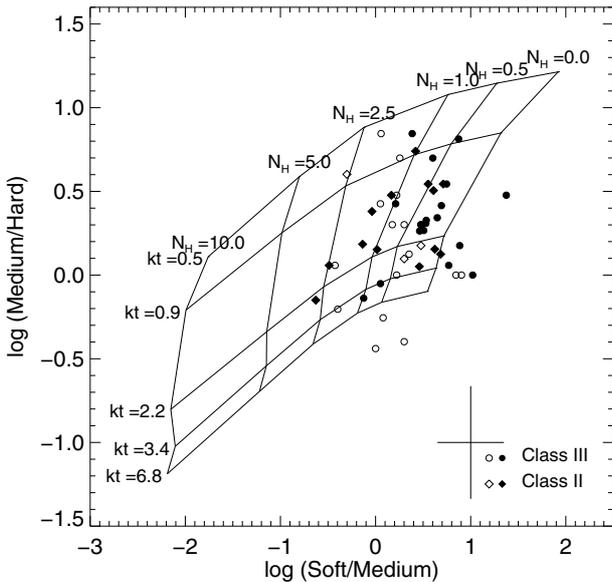
Fig. 3. X-ray hardness ratio diagram for the detected sources; see text in Sect. 2 for a definition of the energy bands. The grid represents the predicted colors for isothermal Raymond-Smith models in a range of temperatures (in units of keV) and affected by different amounts of absorption (in units of 10^{22} cm^{-2}). The YSO classification from Sect. 5 is anticipated here to show the trend for different absorption between Class II and Class III stars. X-ray sources with more and less than 20 net source counts, respectively, are shown with open and filled plotting symbols. A typical error bar is shown in *the lower right*.

differences can probably be ascribed to additional absorbing material in the circumstellar environment of Class II stars. The median temperatures are $(kT)_{\rm C\,II} = 1.5$ keV and $(kT)_{\rm C\,III} = 1.9$ keV for Class II and III, respectively. A difference in kT between these two groups is not expected. We refrain from analyzing its significance because the X-ray luminosity depends very little on the temperature in this range.

With the values of $N_{\rm H}$ and kT described in the previous paragraph, a count-to-flux conversion factor is obtained for each X-ray source with PIMMS[2] from a one-temperature Raymond-Smith model. The corresponding X-ray luminosities are given in Col. 9 of Table 2. Evidently, these numbers are associated with large errors.

As an alternative, we apply also a different method to derive the column density, by computing individual $N_{\rm H}$ estimates based on the $A_{\rm V}$ of each star using a gas-to-dust conversion law of $N_{\rm H} = 1.8\,A_{\rm V}$ [mag]$\times 10^{21}$ cm^{-2} (e.g. Predehl & Schmitt 1995). Note that the $N_{\rm H}/A_{\rm V}$ ratio may vary for different star-forming environments as shown by Vuong et al. (2003), but an assessment of its value in NGC 7129 is out of the reach with the presently available data. The optical extinctions are obtained from deredening of the objects in the J vs. $J - H$ diagram, and is, obviously, only available for X-ray sources with near-IR photometry. A comparison of the X-ray luminosity functions derived with these two approaches is given in Sect. 6.3.

3. Infrared catalog (Spitzer and 2 MASS)

NGC 7129 was observed by the *Spitzer* Space Telescope with IRAC in four wavelength bands from 3.6 to 8.0 μm and with MIPS at 24 μm. These observations are part of the *Spitzer* Young Stellar Cluster Survey, initially presented by Megeath et al. (2004) and further analyzed by Gutermuth et al. (2004), Muzerolle et al. (2004), and Gutermuth et al. (2009). Henceforth, we refer to the last paper as G09. The Astronomical Observation Request (AOR) number and dates of the *Spitzer* observations are AOR 3655168 from 2003-12-24 and AOR 3663616 from 2003-12-29.

Our analysis is based on a catalog comprising *JHK* data from 2 MASS and IRAC and MIPS photometry kindly provided by R.Gutermuth prior to publication. The IRAC and MIPS fluxes have been measured by Gutermuth et al. using the photometry

---

[2] The Portable Interactive Multi-Mission Simulator (PIMMS) is accessible at http://asc.harvard.edu/toolkit/pimms.jsp

tool PhotVis, which is based on DAOPHOT routines ported to IDL. The magnitudes were corrected for aperture losses and calibrated using large-aperture measurements of standard stars. The *Spitzer* sources were visually inspected and non-stellar contaminations rejected. To obtain near-IR counterparts to the *Spitzer* sources, G09 matched their positions with 2 MASS using for the cross-identification radius a maximum of 1″ in the case of IRAC and 1.3″ in the case of MIPS. For more details on the IR photometry, see Gutermuth et al. (2004) and G09.

The combined 2 MASS and Spitzer catalog of NGC 7129 contains 7139 objects, of which 5389 are detected in at least one *Spitzer* band and 287 are detected in all four IRAC bands. The catalog includes the YSO classification discussed in detail by G09; see Sect. 5.6.

4. Optical catalog

NGC 7129 is poorly characterized in the optical. We have compiled a list of studies that have identified pre-MS stars in the cluster. This list will be used to provide optical counterparts for the sample of YSOs that we define in Sect. 5.

The bright B-type star SVS 8, the two Herbig stars SVS 7 and SVS 12, and evidence of some other emission line stars were reported by Herbig (1960). Several far-IR sources lack optical counterparts indicating that they are deeply embedded in the reflection nebula. Most optial imaging surveys carried out in NGC 7129 used narrow band filters to search for Herbig-Haro objects (e.g. Strom et al. 1986; Eiroa et al. 1992). Three emission line stars are reported by Miranda et al. (1993) together with four Herbig-Haro objects. Photometric measurements in the *VRI* bands were presented by Magakian et al. (2004) for 22 stars in the central region of the cluster, most of them newly discovered by means of slitless Hα spectroscopy.

5. YSO census in NGC 7129

Our census of the YSO population in NGC 7129 is based on new X-ray and IR data that yield complementary information. We consider as YSOs (1) those X-ray sources that have IR properties compatible with young stars (Sect. 5.2), and (2) those IR objects that show evidence for emission in excess of the photospheric value irrespective of whether they are detected in X-rays or not (Sect. 5.3). The first group comprises, in principle, all types of YSOs from Class 0/I protostars to Class III objects, while the second group is biased against the identification of the diskless Class III objects. Our criteria for the classification of the YSOs on basis of IR photometry are described in Sect. 5.1 followed by the a description of the selected sample (Sects. 5.2 and 5.3). We identify contaminating foreground and background objects in Sect. 5.4 and discuss the completeness and spatial distribution of the sample in Sect. 5.5. In Sect. 5.6 our results are compared to a more complex selection process applied by G09.

5.1. IR classification criteria for YSOs

Color–color diagrams can be used to examine the evolutionary status of YSOs (e.g. Allen et al. 2004) and to find contaminating background objects. Figure 4 shows a selection of color–color diagrams based on IRAC photometry for the NGC 7129 region. We determined the reddening vector for the IRAC bands with the extinction law of Indebetouw et al. (2005). Our first criterion for identifying stars with circumstellar excess emission is based on the [3.6]−[4.5] vs. [5.8]−[8.0] diagram. We consider Class II

candidates all those objects with 1σ error bars contained in the region defined by Caramazza et al. (2008) and shaded in Fig. 4 (see e.g. Megeath et al. 2004; Hartmann et al. 2005, for previous similar definitions for Class II mid-IR colors given in the literature). We consider candidate Class 0/I protostars all those objects with [3.6]−[4.5] > 0.8. As outlined by White et al. (2007), the unambiguous distinction between Class II and Class 0/I is not trivial and requires good SED coverage and information from spectroscopy. Detailed analyses of SEDs for young stars show that there is some overlap of the Class 0/I and Class II populations as far as their IRAC colors are concerned (Caramazza et al. 2008). In fact, it is evident from Fig. 4 that the Class 0/I group may also contain reddened Class II stars. Similarly, some protostars may be located below the chosen cutoff line. The unambiguous distinction of Class 0/I and Class II for NGC 7129 has to be postponed until spectroscopy is available.

In a second step we examined the near-IR photometry. Generally, in near-IR color–color diagrams objects to the lower right of the reddening band are considered to have circumstellar disks responsible for the red excess emission. For the $J - H$ vs. $H - [4.5]$ diagram, we interpolated the reddening law of Rieke & Lebofsky (1985) to the 4.5 μm filter of IRAC. To exclude objects below the dwarf locus and likely from the background we imposed as constraint $J - H > 0.65$. We then added all objects above that line but below the reddening band in the $J - H$ vs. $H - [4.5]$ diagram to the list of Class II candidates. In principle, this diagram does not allow Class II to be distinguished from protostars. However, that none of the IRAC-selected Class 0/I candidates is in the $J - H$ vs. $H - [4.5]$ area shown in Fig. 4 makes us confident that Class 0/I make a very small contribution to the near-IR selected YSO sample. In fact, only one of the 13 Class 0/I candidates selected from the IR catalog on the basis of IRAC colors has JH photometry, and it has $H - [4.5] = 5.8$, thus lying outside the region plotted in the third panel of Fig. 4. (This object is outside the *Chandra* FOV and, therefore, not listed in our data tables.) We conclude that most protostars are too faint for 2 MASS. In fact, in the sample that we use for scientific analysis (see Sect. 5.5), there is none of the Class 0/I sources because we could not determine their mass.

The sample from which our IR selected YSO candidates are drawn consists of the 287 objects with photometry in all four IRAC bands and the 811 objects with photometry at J, H, and [4.5]. Our YSO classification results in 64 Class II candidates and 13 Class 0/I candidates across the field covered by IRAC. The remaining IR sources are mostly not related to NGC 7129 but they include also the Class III cluster members. In Sect. 5.2 we make use of the X-ray data to identify the last ones.

We did not use MIPS data in our classification scheme because the majority of the objects have no 24 μm detection. However, as a cross-check we show in the rightmost diagram of Fig. 4 a color–color diagram with the reddest color available in the IR catalog, [8]−[24]. The Class II and the Class 0/I regions defined by Muzerolle et al. (2004) are highlighted with different gray shades. The agreement between our individual classifications and the highlighted areas is very good. There are only two Class III (or foreground) objects with very red [8]−[24] color such that the MIPS data is inconsistent with our classification from shorter wavelengths. These objects may have transition disks (Class II/III).

5.2. YSO candidates among detected X-ray sources

The X-ray source list (Table 2) was cross-correlated with the 2 MASS point source catalog (Cutri et al. 2003). We computed
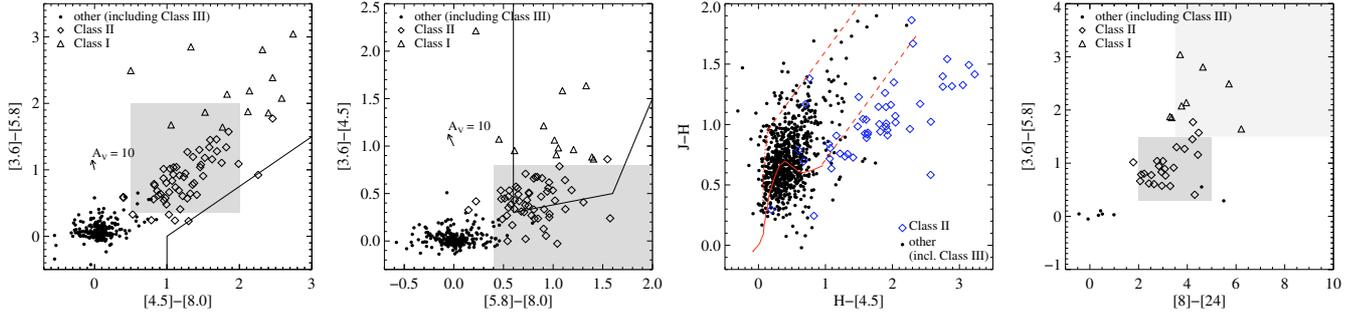
Fig. 4. Color–color diagrams for NGC 7129 based on near-IR and mid-IR photometry. For these plots we used all those *Spitzer* and 2 MASS objects from the catalog described in Sect. 3 that have photometry in the bands defining the displayed colors. The arrows denote reddening vectors with their length corresponding to $A_V = 10$ mag. The solid lines delineate the areas typical for star-forming galaxies (below the line in the first panel) and for broad-line AGN (above the line in *the second panel*), while the shaded areas represent the typical location of Class II YSOs (dark gray) and of Class 0/I YSOs (light gray in the rightmost diagram). Objects classified as Class II and Class 0/I according to the criteria described in Sect. 5.1 are highlighted with different plotting symbols: Class II (diamonds), Class 0/I (triangles), and other IR sources including Class III (circles).

the median position offset between the X-ray sources and their 2 MASS counterparts, and shifted the X-ray positions by this boresight value ($\Delta\alpha = -0.22''$; $\Delta\delta = +0.07''$). For our search radius of $1.5''$ the majority of the X-ray emitters (47/59) have 2 MASS counterparts. Most (43) of these counterparts are found within $<0.5''$ of the X-ray position, and only one counterpart is at $>1''$ from the X-ray position. Then we searched for matches between the X-ray sources and the 2 MASS positions given in the combined 2 MASS/Spitzer catalog introduced in Sect. 3. All but 9 X-ray sources have a mid-IR counterpart in at least one *Spitzer* filter. For the cross-correlation of the X-ray sources with the optical positions from the catalogs described in Sect. 4, we allowed for a maximum matching radius of $2''$. This yielded *VRI* photometry for nine X-ray sources. To this we added the optical photometry for the Herbig star SVS 7 from Hillenbrand et al. (1992) and the one for the B-type star SVS 8 from Racine (1968).

Identifiers from published catalogs and the offset between X-ray and optical/IR sources are listed in Table 3. A compilation of the optical and IR photometry for all X-ray sources in NGC 7129 is given in Table 4. We count 16 Class II and 1 Class 0/I candidates among the X-ray detections. The 30 X-ray sources for which either 2 MASS or IRAC photometry is complete and that are not classified Class 0/I or II are considered Class III candidates. Another 12 X-ray sources remain unclassified. In Col. 13 of Table 4 we report the YSO classification for each individual object. Class II sources with incomplete IRAC photometry and selected only on the basis of near-IR data are labeled with an asterisk. The names of the stars reported in this table go back to various literature sources. Some stars had already been identified in the near-IR survey by Strom et al. (1976). These stars carry "SVS" numbers in Col. 2 of Table 3. Labels "HL85-N" and "HL85-S" refer to the northern and southern fields observed by Hartigan & Lada (1985). "MEG93" stands for Miranda et al. (1993), and "MMN" numbers are stars from Magakian et al. (2004).

Color–color diagrams of the X-ray sources are shown in the left column of Figs. 5 and 6. While Fig. 5 show the diagrams used for the YSO classification, Fig. 6 provides a cross-check of the resulting YSO status in colors not used for the selection process. It demonstrates that our classification is consistent with the expectation from *JHK* photometry (no Class III candidate is in the area for T Tauri stars) and the expectation from MIPS photometry (only one Class III candidate is red at [8]−[24]).

5.3. X-ray undetected YSO candidates

As described in Sect. 5.1 we used the IR photometry to identify YSOs with excess emission from circumstellar disks or envelopes in the *Spitzer* sample. There are 10 Class 0/I and 36 Class II candidates within the *Chandra* FOV but not detected in X-rays. Their optical and IR photometry is summarized in Table 6, where objects are labeled by their running number in the catalog of R. Gutermuth. Similar to the case of the X-ray detected ones, the majority of Class II is selected by their IRAC colors, and only 5 of them (labeled with an asterisk in Col. 14 of Table 6) are classified solely by near-IR photometry. Five stars have optical photometry in the catalogs described in Sect. 4, and *VRI* magnitudes for SVS 12 are extracted from Hillenbrand et al. (1992). The position of the X-ray undetected YSO candidates in the IR color–color diagrams are shown in the right column of Figs. 5 and 6. By definition this sample does not contain Class III stars. Again, our classification scheme is supported by the MIPS data, as the Class 0/I and Class II objects separate according to the empirical locations determined by Muzerolle et al. (2004).

We computed upper limits for the X-ray count rate of the undetected YSO candidates using the algorithm of Kraft et al. (1991). For the conversion into X-ray flux we followed the procedure described in Sect. 2 for the detected sources, i.e. we estimate L_x in two ways: (A) We assumed a 1-T RS-model with kT and N_H corresponding to the median of the values measured in the sample of X-ray detected Class II sources given in Sect. 2, and (B) we adopted for the 1-T model the median kT but individual N_H values for each star obtained from its A_V. Then, for both approaches we computed a count-to-flux conversion factor with PIMMS. The X-ray parameters for the undetected YSO candidates are summarized in Table 5. We discuss the possible effects on the X-ray luminosity upper limits resulting from the assumed column density in Sects. 6.3 and 6.4.

5.4. Contamination of the YSO sample

The IR emitters comprise also extragalactic background objects, galactic background stars, and foreground dwarf stars. Various authors have investigated the position of contaminating background AGN and galaxies in the IRAC color–color diagrams, and we use their results. Stern et al. (2005) have identified an area populated by broad-line AGNs enclosed in the solid line in the [3.6]−[4.5] vs. [5.8]−[8.0] diagram. A brightness cut-off can be used to distinguish AGN from YSO candidates on a
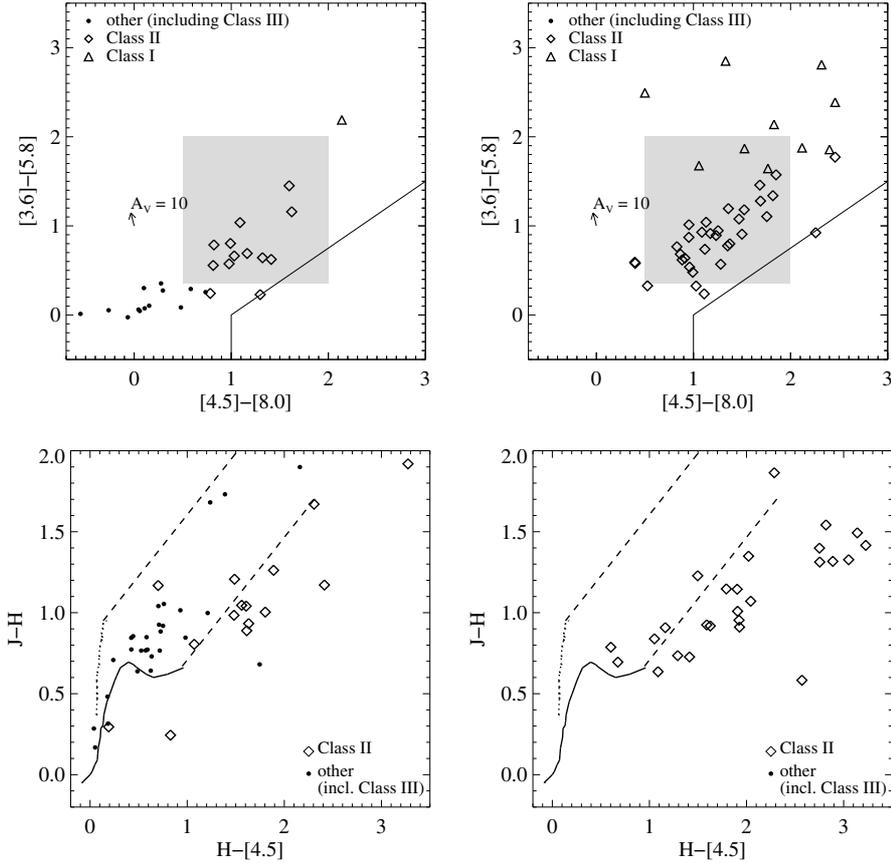
Fig. 5. Color–color diagrams for near-IR and mid-IR photometry used to classify the YSOs: *left* – X-ray sources, *right* – X-ray undetected YSO candidates selected with the criteria described in Sect. 5.1. *In the top row*, the solid line delineates the area of star-forming galaxies (equivalent to the first diagram in Fig. 4). *In the bottom row*, the solid line represents the locus of main-sequence dwarf stars, the dotted line that of giants, and the dashed lines represent the reddening vector.

statistical basis. Star-forming galaxies appear very red at mid-IR wavelengths and are usually found in the lower right area delineated by the solid lines in the [3.6]−[5.8] vs. [4.5]−[8.0] diagram (Gutermuth et al. 2008).

In addition to the region marked by the solid line in the [3.6]−[4.5] vs. [5.8]−[8.0] diagram a brightness limit of [3.6] = 14.5 mag and [4.5] = 14 mag (Jørgensen et al. 2006; Hernández et al. 2007) was used to identify contaminating background AGN. Only two X-ray detected YSO candidates in the highlighted region and 4 undetected YSO candidates are fainter than these magnitudes. They are flagged in Tables 4 and 6. None of these 6 objects has a 2 MASS counterpart, and we consider them likely AGNs. The [3.6]−[5.8] vs. [4.5]−[8.0] diagram demonstrates that none of our YSO candidates is in the area of the extragalactic PAH sources to the right and below the solid line defined by Gutermuth et al. (2008).

The contribution of extragalactic objects to the X-ray emitters can also be estimated from $\log N − \log S$ distributions taking the limiting flux of the observation into account. We use the expression given by Feigelson et al. (2005) to make a rough estimate of the sensitivity limit in the *Chandra* observation. Using the median absorption, $\log N_H$ [cm^{-2}] = 21.4, derived from the hardness ratios of the X-ray sources, we find $f_{x,lim} \sim 7 \times 10^{-15}$ erg/cm^2/s. From the source counts in the *Chandra Deep Field North* (Brandt et al. 2001), we expect ~17 extragalactic objects in the combined ACIS-S2 and ACIS-S3 fields. However, at large off-axis angles, the sensitivity is significantly lower than the number given above, and in practice, most of the

detected X-ray sources are found within or near the 1.7′ cluster core. Thus, the true contamination is likely less. Indeed, most X-ray sources with large distance from the cluster center are not part of the mass limited sample that we define in Sect. 5.5. They have no near-IR photometry from which we could estimate the mass, i.e. they are faint, just as expected for extragalactic objects. For an area the size of the NGC 7129 cluster core only ~1 extragalactic contaminant is predicted. To summarize, both the considerations of the IR colors and magnitudes and the X-ray sensitivity limit indicate that the fraction of AGN and background galaxies among our candidate NGC 7129 members is probably small.

The sample of X-ray selected Class III objects may also contain contaminating objects in the foreground of the cluster. The contribution of foreground field stars can be judged using the results from the *ROSAT*/NEXXUS survey: the typical X-ray luminosity for field stars is $\log L_x$ [erg/s] ~ 28 for F/G dwarfs, ~27.7 for K dwarfs, and ~27 for M dwarfs (Schmitt & Liefke 2004, their Fig.6). Comparing with the average X-ray luminosity in our sample ($\log L_x$ [erg/s] ~ 30), we would thus be able to detect field F/G dwarfs for distances <100 pc, K dwarfs for <70 pc, and M dwarfs for <30 pc. Based on the luminosity function in the solar neighborhood, the space density of dwarf stars peaks in the M dwarf regime at ~0.01 pc^{-3} (Reid & Gizis 1997), and is significantly lower for F/G/K stars (Reid et al. 2002). In the core radius of 1.7′ for NGC 7129, we therefore expect <10^{-5} field stars with detectable X-ray emission. Although this estimate has been derived based on typical numbers, not taking into account
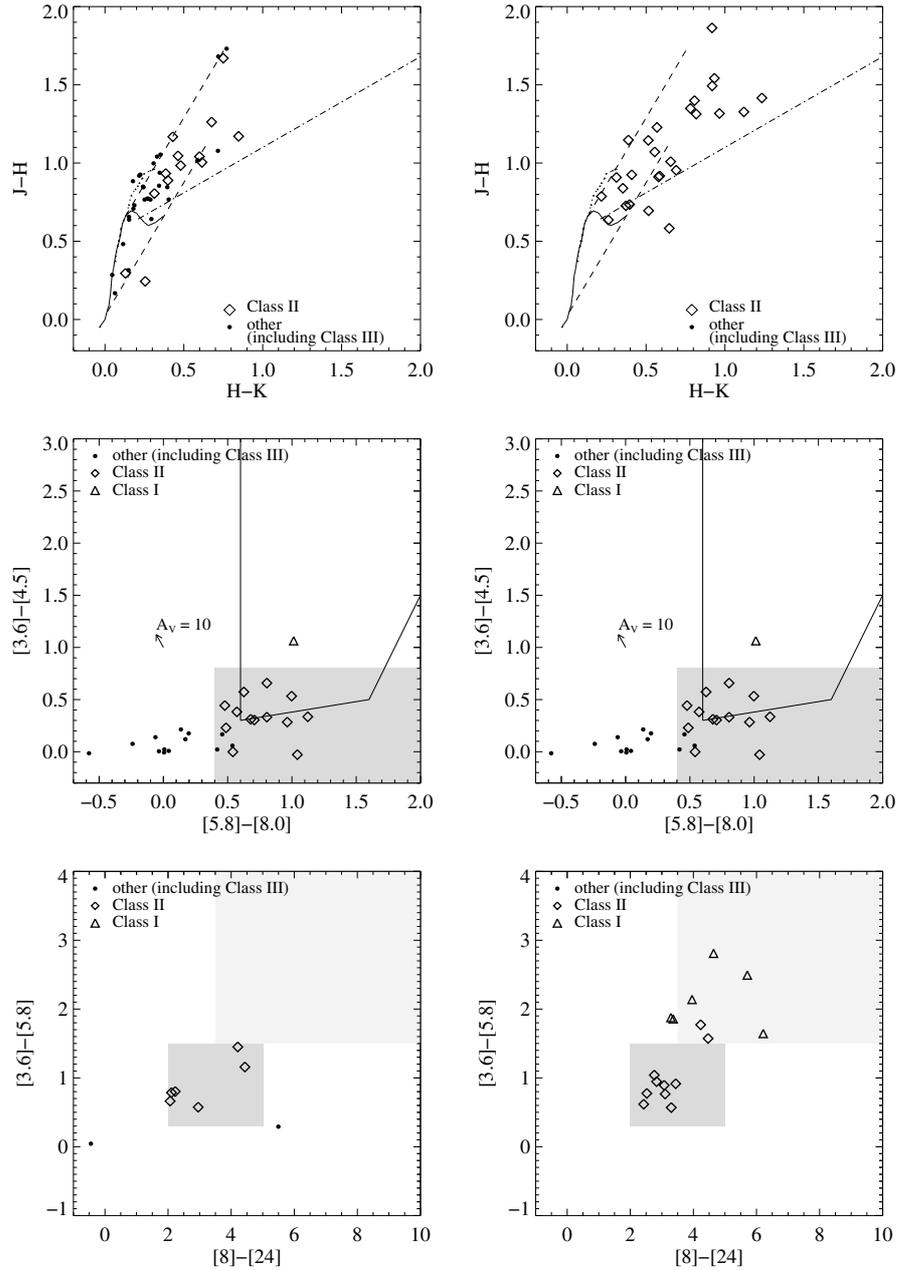
Fig. 6. Additional color–color diagrams for near-IR and mid-IR photometry: *left* – X-ray sources, *right* – X-ray undetected YSO candidates selected with the criteria described in Sect. 5.1. The dash-dotted line in the $J - H$ vs. $H - K$ diagrams represents the locus of classical T Tauri stars from Meyer et al. (1997). See Fig. 4 for the meaning of high-lighted regions.

the significant spread in X-ray luminosities at a given spectral type, the result is safely below 1 and thus negligible.

5.5. Completeness and spatial distribution

For a meaningful comparison of the YSO populations the possible differences in the completeness of X-ray and IR selected samples must be taken into account. In this section we define several sub-samples for NGC 7129 on basis of the stars identified as NGC 7129 candidate members in Sects. 5.1 to 5.4. The selection criteria and the composition of these samples are summarized in Table 1, and the individual stars of each sample are listed in Table 7.

First, we estimate the mass distribution of the YSO candidates from a comparison of their IR photometry with the predictions from evolutionary calculations. We assume a cluster age of 3 Myr and an adequate combination of evolutionary models: Low-mass stars at an age of few Myr are still in their pre-MS phase, and we use the model from Siess et al. (2000) converted to the observational plane using the calibration given by Kenyon & Hartmann (1995). The Siess et al. calculations extend up to $7\,M_\odot$, i.e. they do not cover the full mass range of our sample. For the high-mass stars we use the calculations from Marigo et al. (2008). At the high-mass end of the 3 Myr isochrones the Siess calculations are in good agreement with the Marigo model. Therefore, we use the Siess isochrone for $M \leq 2.7\,M_\odot$ and the Marigo isochrone for higher masses.

**Table 1.** Composition of different subsamples of NGC 7129.

――― Sample characteristics ―――			Class II		Class III		Total	
$M > 0.5\,M_\odot$	$A_V < 5\,$mag	core	N	$(N_{det}/N_{u.l.})$	N	$(N_{det}/N_{u.l.})$	N	$(N_{det}/N_{u.l.})$
√			26	(13/13)	25	(25/0)	51	(38/13)
√	√		13	(9/4)	21	(21/0)	34	(30/4)
√		√	16	(7/9)	16	(16/0)	32	(23/9)
√	√	√	7	(5/2)	14	(14/0)	21	(19/2)

From the J vs. $J - H$ diagram (Fig. 7) it emerges that all X-ray detected stars in NGC 7129 with known J and H magnitudes have $M > 0.3\,M_\odot$ according to the evolutionary calculations. In the Orion nebula cluster (ONC), at 1 Myr just slightly younger than NGC 7129, stars with $\log L_x$ [erg/s] $= 29.9$ corresponding to the sensitivity limit derived in Sect. 5.4, have a mass of $\sim 0.5\,M_\odot$ (Preibisch et al. 2005). Therefore, we take the X-ray sample to be complete down to this mass. About half of the YSOs that are not detected with *Chandra* are fainter in J than predicted for a cluster member of $0.5\,M_\odot$. X-ray non-detected YSOs below the reddening track of an $M > 0.5\,M_\odot$ star according to the Siess et al. (2000) model are dropped from the sample for further analysis.

Obviously, the sample defined this way comprises only stars with available photometry in the J and H bands. This is not a serious limitation because *Spitzer* sources without known JH magnitude are likely fainter than our mass cutoff. The resulting sample consists of 38 X-ray sources (13 Class II and 25 Class III) and 13 X-ray undetected Class II YSOs selected from their *Spitzer* colors; see first row in Table 1. By introducing this sensitivity cutoff the four AGN candidates discussed in Sect. 5.4 are also dropped. No Class 0/I sources are in the mass-limited sample because none of them have JH photometry.

There is evidence of higher average extinction in the YSO sample that have X-ray upper limits with respect to the sample of X-ray sources (see Figs. 7 and 6 top panel). About half of the Class II stars are in the upper limit sample, while Class III stars are by definition present only in the X-ray detected sample. This might imply that the sensitivity limit is different for the two object groups. Class III sources with large extinction may, indeed, be absent from the sample because high column density impedes the X-ray photons from being observed. To eliminate a possible bias, we define a "lightly absorbed" sample limited by $A_V < 5\,$mag. There are very few X-ray undetected YSOs with low extinction above our mass cutoff (Fig. 7 bottom), supporting our estimate that the X-ray observation is (nearly) complete down to $0.5\,M_\odot$. The mass-limited, lightly absorbed sample consists of 13 Class II sources (4 of which not detected in X-rays) and 21 Class III sources; second row in Table 1.

We move on now to consider the spatial distribution of the YSO population in NGC 7129. Gutermuth et al. (2004) noticed that there is an accumulation of Class II YSOs around SVS 12, at the outskirts of and pointing away from the molecular cloud. This is also the direction where most X-ray sources are found, apart from those in the cluster core. A map with the cloud contours and our mass-limited sample is shown in Fig. 8. To eliminate effects related to a possible difference in the spatial distribution of YSOs in different evolutionary stages, we define a sample limited by the cluster core radius as described by Gutermuth et al. (2004), henceforth called the "core sample". The mass limited core sample is composed of 23 X-ray emitters, of which 7 are Class II objects and 16 are Class III. These numbers represent a fraction of 44% and 53% of the total sample of X-ray detections for Class II and Class III, respectively (cf.
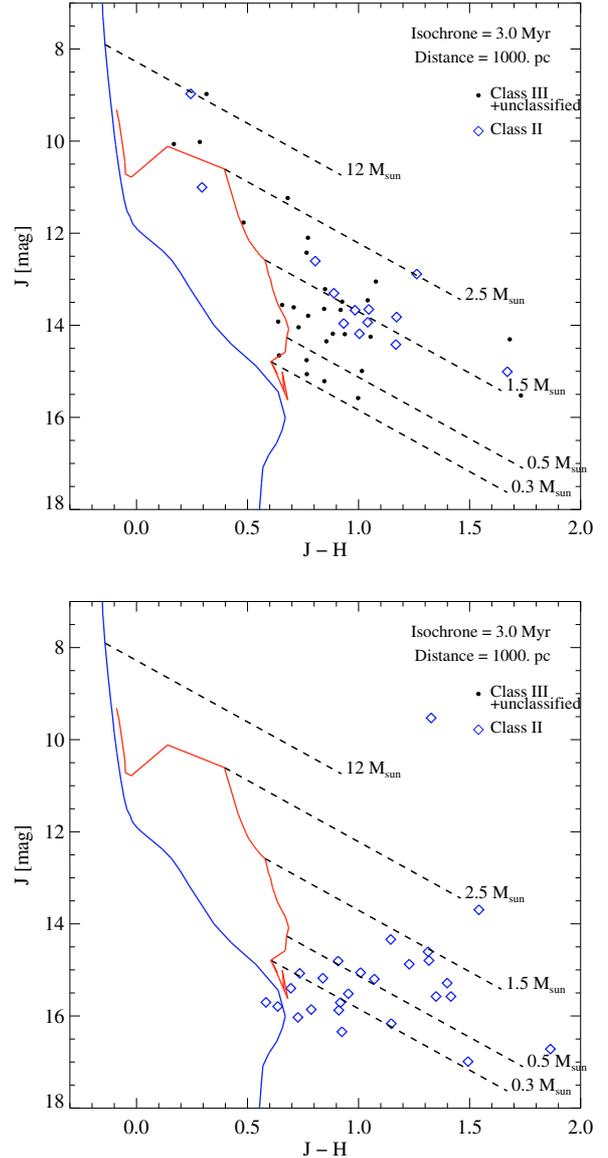
Fig. 7. J vs. $J - H$ diagram for the 2 MASS photometry of X-ray detected (*top*) and non-detected (*bottom*) cluster candidates in NGC 7129. The two solid lines represent the 3 Myr isochrone for the pre-MS calculations from Siess et al. (2000) (*right*, red line) and the calculations from Marigo et al. (2008) (*left*, blue line), respectively. The dashed lines indicate the reddening vector for a 0.3, 0.5, 1.5, 2.5, and 12 $M_\odot$ star following Rieke & Lebofsky (1985). Their length corresponds to a visual extinction $A_V = 10\,$mag.

Table 4). The mass-limited core sample, therefore, seems to reflect roughly the spatial distribution of X-ray bright Class II and Class III in NGC 7129. In addition to those 23 X-ray sources, the mass-limited core sample includes 9 Class II objects not detected
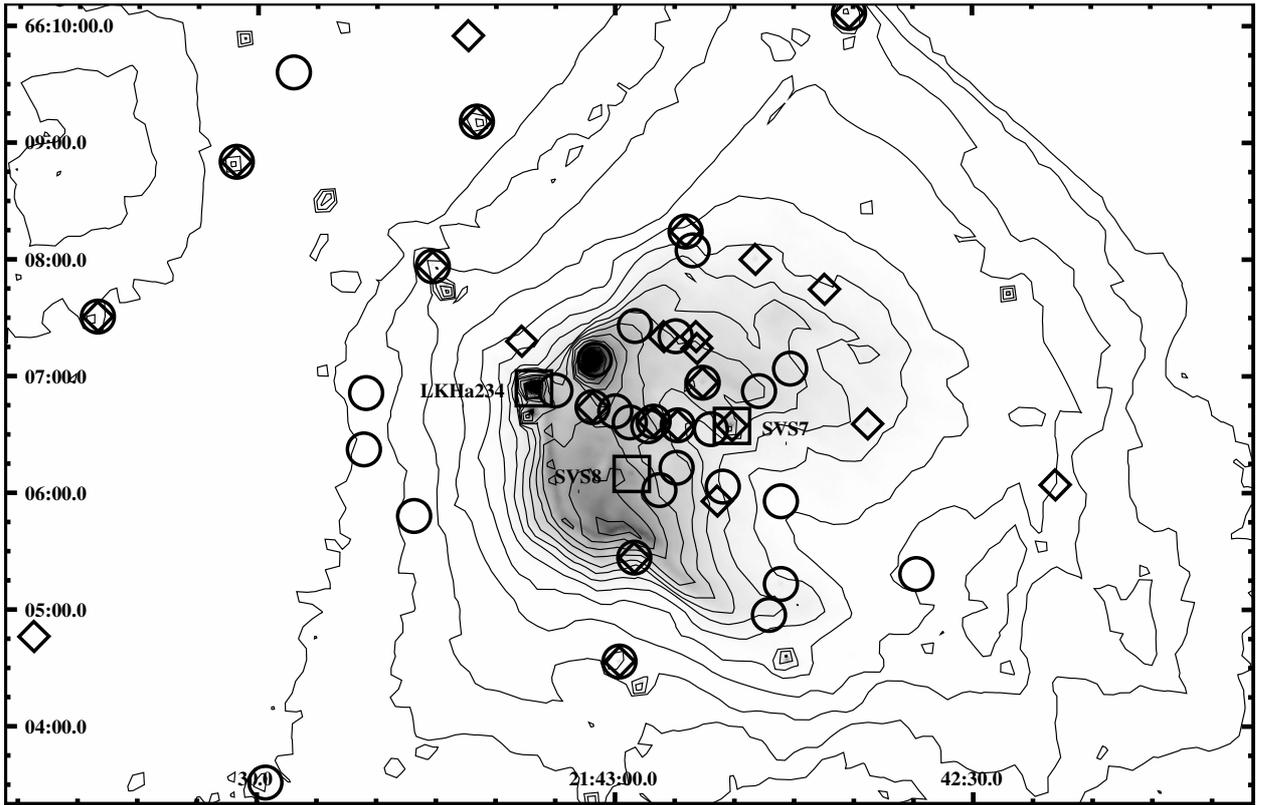
Fig. 8. Contour plot for the IRAC 8 μm image of NGC 7129 from Program # 6 with PI Fazio. Contour levels go from 5 to 1000 MJy/sr in logarithmic steps. Squares show the position of the three hot stars. Circles are X-ray sources and diamonds are YSO candidates identified on basis of near-IR/mid-IR emission irrespective of whether detected in X-rays. Only stars from the mass limited sample defined in Sect. 5.5 are shown. One X-ray detected and one non-detected member of this sample are outside the field shown in the figure.

with *Chandra* (see third row in Table 1). Finally, for the reasons outlined above, we apply an extinction cutoff to this sample. This defines the most restricted sample used in this work, the mass-limited, lightly absorbed core sample. It comprises 7 Class II (of which 2 undetected in X-rays) and 14 Class III, and is summarized in the last row of Table 1.

5.6. Comparison to the classification scheme of Gutermuth et al.

Gutermuth et al. (2008) have devised a complex scheme for the classification of YSOs that was subsequently revised and applied to a wide range of nebulous star-forming environments (G09). In this scheme the distinction between Class 0/I and Class II sources is based on the [4.5]−[5.8] color rather than on the [3.6]−[4.5] color, thus reducing effects of the reddening that are more severe at shorter wavelengths (Flaherty et al. 2007). In a second step, the near-IR photometry is used to deredden the stars and to identify excess emission at wavelengths shorter than [5.8]. Finally, G09 use MIPS photometry to identify deeply embedded protostars without detectable emission in the IRAC bands. We refer to G09 for details of the procedure. Here, we present a brief comparison of the results for the case of NGC 7129.

Overall, we found our classification scheme to be consistent with the more exhaustive approach used by G09. Specifically, most of the objects classified as probably extragalactic are common to both studies. Among the 9 Class 0/I candidates in our list, 5 are classified Class I by G09, one is Class 0, one is Class II and two are flagged as shock sources. Better agreement is found for the Class II and Class III samples that are more relevant to

our study than the protostars. In particular, the mass-limited and the core sample defined in Sect. 5.5 are very clean. Our Class II core sample only comprises two objects that carry different flags in the scheme of G09 (one detected in X-rays and one not detected). Conversely, G09 assign Class II status to three X-ray undetected objects in the cluster core that are not identified as YSOs by our procedure. One of them has no 2 MASS photometry, and would not have been selected in our mass-limited sample. Therefore, the Class II sample size is almost identical for the two selection approaches. In the framework of this paper, an accurate YSO classification is relevant only for the evaluation of the disk fraction, and in practice, the differences are not significant (see Sect. 6.2).

6. Results

6.1. SEDs

We examined the SEDs of all sources from Tables 4 and 6. Due to the limited spectral range covered by the available photometry of most sources we abstained from a systematic analysis and searched only for outstanding objects. In particular, we were interested in identifying objects with "holes" in the SED (i.e. excess emission is only visible at the longest wavelengths) and embedded objects or objects with edge-on disks (i.e. with strongly increasing flux levels towards longer wavelengths). This exercise was limited to sources for which the data cover at least the wavelength range from 1.25 to 8 μm with a minimum of 6 datapoints. These limits were imposed to guarantee a minimum amount of
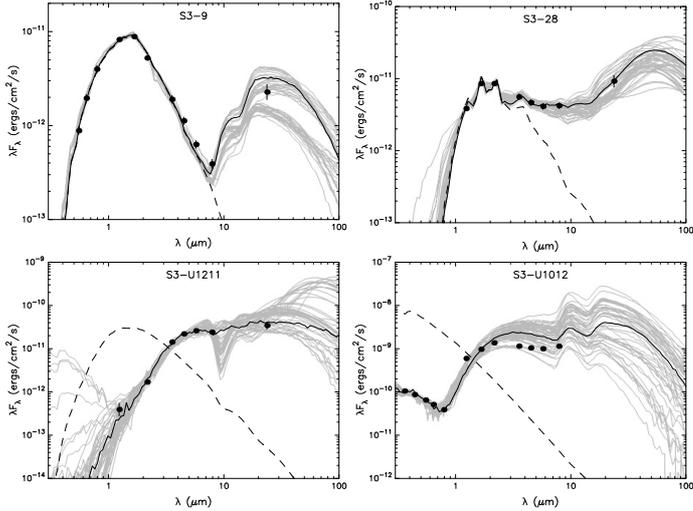
Fig. 9. Observed SEDs (datapoints) for four "peculiar" objects together with their 50 best fitting model SEDs from the grid computed by Robitaille et al. (2006, 2007). The best fitting model is shown as black solid line. The dashed line shows the photospheric spectrum without obscuration by disk or envelope, but with interstellar reddening.

information about both the stellar photosphere and the circumstellar environment.

Three objects clearly stand out based on their SED characteristics: NGC 7129-S3-X28 and NGC 7129-S3-X9 from the X-ray detected sample, and NGC 7129-S3-U1211 from the non-detections in X-rays. These objects were selected for further analysis. We added object NGC 7129-S3-U1012 (identified with the Herbig star LkHα 234), which is the brightest source in our sample at all IRAC wavelengths.

For these four objects we compare the observed SED with the grid of model SEDs, pre-computed using a Monte Carlo radiation transfer code, provided by Robitaille et al. (2006, 2007)[3]. Interpreting SEDs using radiative transfer code is subject to degeneracies, as discussed in detail in the literature (Chiang et al. 2001). Spatially resolved multi-wavelength observations can break the degeneracies (Watson et al. 2007) but are only available for relatively few objects. Therefore, we do not attempt to derive a unique model solution for the observed SED. Instead, the following analysis is based on the 50 best-fitting models according to χ^2 for each object, selected from a grid of 200 000 pre-computed YSO models. For more information on the specifications and limitations of the model grid see Robitaille et al. (2006, 2007). In Fig. 9 we show the observed SEDs and the 50 best fitting models for each of the four stars. We have applied generic errors of 10% for all IRAC fluxes and 20% for all MIPS fluxes to account for calibration uncertainties. (These errors are significantly higher than the nominal errors in all cases.) As can be seen, all four objects are adequately matched by a significant number of models.

The multi-parameter fit produces partly ambiguous results, so we limit the discussion to those parameters that are well-constrained by the procedure. While the near-IR photometry mostly constrains the photospheric properties of the central objects, the fluxes at mid-IR wavelengths are strongly sensitive to the inner disk geometry, i.e. flaring, inclination, inner disk radius. In addition, the fluxes in our wavelength coverage are affected by the accretion rate. At $24 \, \mu$m the envelope begins to

---

[3] The SED fitter is available under http://caravan.astro.wisc.edu/protostars/

contribute significantly, thus allowing us to constrain the evolutionary state of the object. The lack of longer wavelength data precludes putting limits on global parameters of disk and envelope (see Wood et al. 2002, for further information). In the following we briefly discuss the results for each of the four objects shown in Fig. 9. The limitations of the model fit (e.g. finite resolution and parameter coverage of the grid) sometimes do not allow a perfect fit of all datapoints. These type of models also do not take variability or 3D structure in the disk into account.

Source NGC 7129-S3-X9 is identified with an Hα emission line star ($W_{\mathrm{H}\alpha}$ = 9.8 Å, see Magakian et al. 2004). Optical photometry in *VRI* bands is available, which has allowed us to estimate the mass of the central source, which is around $1 \, M_\odot$ ($0.4 - 2 \, M_\odot$). NGC 7129-S3-X9 does not show IR excess for $\lambda < 6 \, \mu$m, but a strong excess level is seen at $24 \, \mu$m. This is the hallmark sign of a disk with an inner opacity hole, often called "transition disk" in the literature. Indeed, in its broadband shape, this SED resembles the ones measured for TW Hya (Calvet et al. 2002) and CoKu Tau/4 (D'Alessio et al. 2005). Possible explanations for opacity holes include the presence of a massive planet or a stellar companion. The best-fitting SED models give an inner disk radius of 10 AU ($4 - 30$ AU). This is $\sim$100 times larger than the sublimation radius that usually limits the extent of the inner dust disk.

The SED for object NGC 7129-S3-X28 significantly increases between 8 and $24 \, \mu$m. The datapoints are well-reproduced by models for a disk with a high degree of flaring (i.e. the scale height increases strongly with increasing distance from the star) embedded in an envelope. The best estimate for the mass of the central object is $0.1 - 0.6 \, M_\odot$ but optical photometry is required for a more reliable assessment. The high $24 \, \mu$m flux indicates that this object is possibly in an early evolutionary state. Indeed, in the [3.6]−[5.8] vs. [8]−[24] diagram it is just at the intersection between the canonical areas for Class II and Class 0/I objects.

Object NGC 7129-S3-U1211 has been classified as Class 0/I source in Sect. 5.3. This is confirmed by the SED fit. This is one of the objects with the steepest SED slope in our sample. The flux levels increase steeply from near-IR wavelengths to $24 \, \mu$m. For this object, most parameters are poorly constrained. As can be seen in the plot, the photospheric fluxes are strongly suppressed by circumstellar extinction. Optical and submillimeter measurements would permit putting more reliable limits on the physical properties of the source.

For NGC 7129-S3-U1012 (alias SVS 12) optical *UBVRI* photometry was presented by Hillenbrand et al. (1992) in their study of Herbig stars. These data are combined with 2 MASS and IRAC photometry in Fig. 9. The 50 best-matching SEDs constrain the mass of the central object to $5 - 15 \, M_\odot$. Most of the best-fitting models have a disk inclination $>75°$, i.e. close to edge-on. The disk thus suppresses the observable photospheric flux responsible for the optical emission. It may even be conjectured that the non-detection of SVS 12 in X-rays results from the absorption of its coronal emission. Recall, however, that the presence of an X-ray production mechanism on Herbig stars is not obvious; we refer to Stelzer et al. (2009) for more details on this subject.

6.2. Disk fraction

In the total sample of YSOs for which a mass could be estimated from the J vs. $J − H$ diagram, we count 26 Class II objects and 25 Class III objects (see first row of Table 1). This corresponds to a disk fraction of 51 ± 14%. The uncertainty represents the

95% confidence limit for a binominal distribution. Considering only the mass-limited core sample there are 16 Class II and 16 Class III objects. Therefore, the disk fraction for the core of NGC 7129 is 50±18%. In the mass-limited lightly absorbed core sample, there are 7 Class II and 14 Class III sources, and we derive a disk fraction of $33^{+24}_{-19}\%$. We recall that this last sample is the least biased one but, obviously, also the least complete one in terms of number of cluster members.

Gutermuth et al. (2004) have estimated the fraction of disk-bearing stars in the core of NGC 7129 using a sample selected from the $J - H$ vs. $H - [4.5]$ diagram with a brightness ($J <$ 15.5 mag) and extinction ($A_V < 6$ mag) cutoff. With help of a control field they estimated that 20% in the sample without IR excess emission are background objects, and derive a disk fraction of $54 \pm 14\%$. This number is statistically similar to the value obtained for our mass-limited core sample without an extinction cutoff. For the absorption limited case we obtain a smaller disk fraction than Gutermuth et al. (2004). The use of X-ray emission as a diagnostic for identifying the young disk-less population allows us to reduce the uncertainties due to background contamination. There are no significant differences in the derived disk fraction between our YSO classification method and the more sophisticated approach of G09. Using their YSO status together with our sample restrictions (mass-limit, extinction limit and confinement in the core), we find a disk fraction of $39^{+25}_{-22}\%$.

We compared the disk fraction in NGC 7129 with literature values for other clusters and star-forming regions in the same age range. Given the possibility of a mass dependence in the disk lifetimes, care has to be taken to compare similar mass regimes. The majority of the sources in NGC 7129 have masses between 0.5 and 2.5 $M_\odot$ (see Fig. 7). For consistency, we limit ourselves to disk fractions estimated with *Spitzer*/IRAC data.

In Cha I (~2 Myr), the disk fraction is roughly at 50% with an error bar of ±6% from 0.1 to 3 $M_\odot$ (Damjanov et al. 2007; Luhman et al. 2008). This sample is dominated by stars with sub-solar masses and there are indications that the number is some-what higher for $M > 1 M_\odot$. In the cluster IC 348, at 2−3 Myr, the total fraction of objects harboring disks is 50±6%. Here the stars with $M > 1 M_\odot$ have a significantly lower disk fraction of ~20% (Lada et al. 2006). The cluster σ Ori with an estimated age of 3 Myr has been found to have a disk fraction of 36±4% for stars with $0.1 < M < 1 M_\odot$, and 27 ± 7% for 1−2 $M_\odot$ (Hernández et al. 2007). Finally, the disk fraction in the 5 Myr old Upper Sco star-forming region is ~19% for $0.1-1 M_\odot$, and close to zero for higher mass stars (Carpenter et al. 2006).

As seen from this list, the disk fraction declines steeply with age between 1 and 5 Myr (see also Haisch et al. 2001). The value we derived for the disk fraction of the absorption limited core sample of NGC 7129 with $M > 0.5 M_\odot$ is clearly higher than in Upper Sco and lower than in Cha I and IC 348. Therefore, the age of NGC 7129 is probably in between that of those regions, and similar to σ Ori, i.e. ~3 Myr.

6.3. X-ray luminosity functions

Using the ASURV environment (Feigelson & Nelson 1985), we computed the XLF for the two core samples of NGC 7129, the mass-limited and the mass- and absorption-limited one. Three stars with $J < 10.0$ mag are not considered in this part of the analysis as they are hot stars according to Fig. 7 and their X-ray emission may originate not in the corona but in winds. The two X-ray detected hot stars are identified with the dominating B-type stars of the reflection nebula, SVS 8 and SVS 7, and
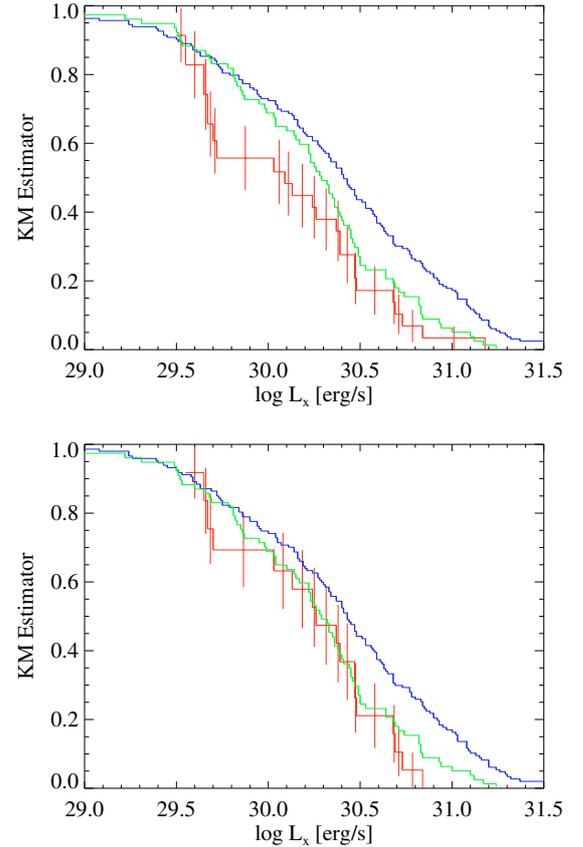
Fig. 10. X-ray luminosity functions for the core sample of NGC 7129 (red, with error bars) compared to the distributions for the ONC (blue, rightmost line) and NGC 2264 (green). The ONC and NGC 2264 comprise the mass range $0.5 > M > 2.5 M_\odot$. The NGC 7129 distributions are composed from the X-ray luminosities derived with the N_H values obtained from the X-ray hardness ratios (see Sect. 2). *In the top panel* we show the mass-limited core sample, while in *the bottom panel* an extinction cutoff was introduced ($A_V < 5$ mag).

the hot star not detected with our algorithm is the Herbig star SVS 12. The X-ray emission of all three stars was discussed in detail by Stelzer et al. (2009).

The XLF for the mass-limited core sample of NGC 7129 with X-ray luminosities using the N_H obtained from the hardness ratios is shown in the top panel of Fig. 10. Without the three hot stars this sample consists of 29 stars composed of 15 Class III and 14 Class II sources. Eight of the latter ones have X-ray upper limits. The median X-ray luminosity is $(\log L_x)_{med}$ [erg/s] = 30.1. For comparison we also show the XLF for two other samples of young stars, the ONC and NGC 2264. The data for the ONC were extracted from the *Chandra Orion Ultradeep Project* (COUP) (see Getman et al. 2005b). After eliminating the probable nonmembers identified by Getman et al. (2005a) from the COUP source list, we limited the XLF of the ONC to stars with masses in the range $0.5...2.5 M_\odot$. As described in Sect. 5.4, this is the approximate mass range covered by the NGC 7129 sample. Similarly, the XLF of NGC 2264 shown in green in Fig. 10, obtained with data from Flaccomio et al. (2006), is restricted to stars with spectroscopically determined masses between 0.5 and 2.5 $M_\odot$. In this mass range, the median X-ray luminosity for the ONC is $(\log L_x)_{med}$ [erg/s] = 30.4 and for NGC 2264 it is $(\log L_x)_{med}$ [erg/s] = 30.3. The precise choice of the upper mass bound for the two comparison clusters is not a concern. We

Table 7. Composition of the subsamples described in Sect. 5.5.

NGC 7129-...	$M > 0.5\,M_\odot$	$M > 0.5\,M_\odot$ in core	$M > 0.5\,M_\odot$ in core $A_V < 5$ mag
...-S3-X1	√		
...-S3-X2	√		
...-S3-X3	√		
...-S3-X4	√		
...-S3-X6	√	√	√
...-S3-X9	√		
...-S3-X10	√	√	√
...-S3-X11	√	√	√
...-S3-X13	√	√	√
...-S3-X14	√		
...-S3-X15	√	√	√
...-S3-X16	√	√	√
...-S3-X17	√	√	√
...-S3-X18	√	√	√
...-S3-X19	√	√	√
...-S3-X20	√	√	√
...-S3-X21	√		
...-S3-X22	√	√	
...-S3-X23	√	√	√
...-S3-X25	√	√	
...-S3-X26	√	√	√
...-S3-X28	√		
...-S3-X29	√	√	√
...-S3-X30	√		
...-S3-X31	√	√	√
...-S3-X32	√	√	√
...-S3-X35	√	√	√
...-S3-X36	√	√	√
...-S3-X40	√	√	√
...-S3-X43	√	√	
...-S3-X45	√	√	
...-S3-X51	√	√	√
...-S3-X52	√		
...-S3-X56	√		
...-S2-X1	√		
...-S2-X4	√		
...-S2-X5	√		
...-S2-X9	√		
...-S3-U815	√	√	√
...-S3-U840	√		
...-S3-U939	√	√	
...-S3-U1012	√	√	
...-S3-U1085	√	√	
...-S3-U1103	√	√	
...-S3-U1107	√	√	
...-S3-U1109	√	√	√
...-S3-U1194	√	√	
...-S3-U1246	√	√	
...-S2-U613	√		
...-S2-U820	√		
...-S2-U1640	√		

lowered it to $2.0\,M_\odot$ and found no dramatic change of the median X-ray luminosities.

In the lower panel of Fig. 10 we show the mass-limited lightly absorbed core sample of NGC 7129 together with the ONC and NGC 2264 samples to which the same restrictions have been applied (i.e. mass range of $0.5...2.5\,M_\odot$ and $A_V < 5$ mag). The median X-ray luminosity for this NGC 7129 sample is higher than for the one without limitations on the absorption $((\log L_x)_{med}\,[\mathrm{erg/s}] = 30.3)$ because it has fewer upper limits. For the ONC less than 10% of the sample is removed due to the absorption cutoff, and there is no change in the median L_x. In NGC 2264 all stars have $A_V < 5$ mag.

As mentioned in Sect. 2 the column densities (derived from the hardness ratios) that are used to compute the X-ray luminosities are associated with large uncertainties, and as a cross-check we applied an independent method to derive N_H values from the optical extinction extracted from near-IR photometry. The XLF

for the mass-limited core sample and for the mass-limited lightly absorbed core sample of NGC 7129 computed with those latter N_H estimates both have a median of $(\log L_x)_{med}\,[\mathrm{erg/s}] = 30.2$. This shows that the XLF are relatively stable despite the considerable uncertainties in the computation of the luminosities.

Various uncertainties are related to the calculation of the XLFs, such that the similarity to that of the other clusters is remarkable. We can speculate on the origin of the remaining differences. A possible contribution is from the uncertain mass estimates by means of photometric observations. In addition, the uncertain distance estimate for NGC 7129 may play a role. To bring its XLF up by a factor ~2, the distance would have to be 1.4 kpc instead of the canonical value of 1 kpc. While this does not seem impossible, an investigation of the consequences (that include a higher mass limit for our observations) is clearly unfeasible with the presently available data. Spectroscopic observations of NGC 7129 will shed light on this issue.

6.4. X-ray emission from protostars

None of the Class 0/I candidates is detected in X-rays. The only X-ray detected object classified Class 0/I according to our IR selection does not survive our contamination tests and is flagged as AGN in Table 4. We derived upper limits on the order of $\log L_x\,[\mathrm{erg/s}] \sim 29.5...30.0$ for the undetected Class 0/I candidates. However, the extinction of these embedded objects is likely to be much higher than the assumed median of the X-ray detected Class II sources, and consequently the X-ray luminosities are probably higher than estimated. For $A_V = 15$ mag, a moderate absorption for a protostar, the gas column density is expected to be $\log N_H\,[\mathrm{cm^{-2}}] \sim 22.4$, and the upper limits to the X-ray luminosities higher by a factor four with respect to the values given in Table 5, i.e. $\log L_x\,[\mathrm{erg/s}] \sim 30.1...30.6$. This is in the middle of the range of X-ray luminosities for Class 0/I sources seen in the ONC (Prisinzano et al. 2008). Therefore, the non-detection of most Class 0/I sources in NGC 7129 is not surprising. There is also no X-ray source at the position of the Class 0 object FIRS-2.

7. Summary

We present a combined X-ray and near/mid-IR census of the young star cluster associated with the reflection nebula NGC 7129. YSOs are characterized by excess emission in the IR due to the presence of disks and elevated levels of X-ray emission due to enhanced coronal activity compared with field stars. Thus, the two wavelength regimes provide complementary information that should allow us to obtain a complete census of the cluster population.

In a 22 ks long *Chandra* observation pointed at the Herbig star SVS 12, we find a total of 59 X-ray sources, from which 47 are matched with 2 MASS photometry. Fifty X-ray sources have counterparts seen in at least one IRAC or MIPS band in the *Spitzer* catalog kindly provided to us by Gutermuth (see also G09).

Based on recommendations in the literature, we define a set of criteria to distinguish between Class I/II objects (with disks and/or envelope) and diskless Class III objects from their color in IRAC and 2 MASS photometry. For Class III candidates we require, besides their detection in X-rays, that either the 2 MASS or IRAC photometry is complete. After likely extragalactic sources have been removed, there are 0 Class 0/I, 15 Class II and 30 Class III candidates among the X-ray detections. In addition,

we have identified 8 Class 0/I candidates and 34 Class II candidates without X-ray detection in the *Spitzer*/2 MASS catalog.

Based on a comparison with evolutionary tracks, we estimate that this sample is complete down to $0.5\,M_\odot$. The mass-limited census ($M > 0.5\,M_\odot$) is composed of 26 Class II and 25 Class III objects, from which 16 Class II, and 16 Class III are densely clustered within $1.7'$ around the center of the cloud. The sample may not be complete for strongly absorbed cluster stars. Therefore, we defined an absorption limited subsample, that comprises 7 Class II and 14 Class III sources. Spectroscopy is required to further assess the completeness and properties of this sample.

From our census, we estimate the disk fraction in NGC 7129 to be ~33%. This is lower than the disk fraction of Cha I and IC 348 (2−3 Myr), higher than the disk fraction of Upper Sco (5 Myr), and comparable with the disk fraction of σ Ori (3 Myr). Therefore, the age of NGC 7129 is likely to be ~3 Myr. The same age is suggested by the XLF that we find to be similar to that of the 3 Myr old NGC 2264 cluster but fainter than for the ONC (1 Myr).

For both methods used to derive the luminosities, the XLF of the mass-limited core sample in NGC 7129 are somewhat lower than those of NGC 2264 and the ONC. Better agreement with NGC 2264 is obtained for the lightly absorbed mass-limited core sample, indicating that this sample is likely representative for the cluster.

Based on the broadband shape of their SED, we identify four peculiar sources. Further analysis using the grid of model SEDs by Robitaille et al. (2006) reveals that one object is a clear candidate for a "transition" disk with an inner opacity hole (radius 10 AU). For the well-known HAeBe star LkHα 234 we find evidence for an edge-on disk which blocks the optical light from the central object.

The presently available data set is subject to various uncertainties related with the cluster properties (such as mass distribution or distance) and with the X-ray data itself (such as the spectral shape of the sources). This underlines the need to characterize the cluster members with optical photometric and spectroscopic observations.

References

Albacete Colombo, J. F., Flaccomio, E., Micela, G., Sciortino, S., & Damiani, F. 2007, A&A, 464, 211

Allen, L. E., Calvet, N., D'Alessio, P., et al. 2004, ApJS, 154, 363

Bechis, K. P., Harvey, P. M., Campbell, M. F., & Hoffmann, W. F. 1978, ApJ, 226, 439

Brandt, W. N., Alexander, D. M., Hornschemeier, A. E., et al. 2001, AJ, 122, 2810

Cabrit, S., Lagage, P.-O., McCaughrean, M., & Olofsson, G. 1997, A&A, 321, 523

Calvet, N., D'Alessio, P., Hartmann, L., et al. 2002, ApJ, 568, 1008

Caramazza, M., Micela, G., Prisinzano, L., et al. 2008, A&A, 488, 211

Carpenter, J. M., Mamajek, E. E., Hillenbrand, L. A., & Meyer, M. R. 2006, ApJ, 651, L49

Chiang, E. I., Joung, M. K., Creech-Eakman, M. J., et al. 2001, ApJ, 547, 1077

Cutri, R. M., Skrutskie, M. F., van Dyk, S., et al. 2003, 2MASS All Sky Catalog of point sources, The IRSA 2MASS All-Sky Point Source Catalog, NASA/IPAC Infrared Science Archive, http://irsa.ipac.caltech.edu/applications/Gator/

D'Alessio, P., Hartmann, L., Calvet, N., et al. 2005, ApJ, 621, 461

Damjanov, I., Jayawardhana, R., Scholz, A., et al. 2007, ApJ, 670, 1337

Eiroa, C., Gomez de Castro, A. I., & Miranda, L. F. 1992, A&AS, 92, 721

Eiroa, C., Palacios, J., & Casali, M. M. 1998, A&A, 335, 243

Evans, N. J., Dunham, M. M., Jørgensen, J. K., et al. 2009, ApJS, 181, 321

Feigelson, E. D., & Nelson, P. I. 1985, ApJ, 293, 192

Feigelson, E. D., Getman, K., Townsley, L., et al. 2005, ApJS, 160, 379

Flaccomio, E., Micela, G., & Sciortino, S. 2006, A&A, 455, 903

Flaherty, K. M., Pipher, J. L., Megeath, S. T., et al. 2007, ApJ, 663, 1069

Font, A. S., Mitchell, G. F., & Sandell, G. 2001, ApJ, 555, 950

Freeman, P. E., Kashyap, V., Rosner, R., & Lamb, D. Q. 2002, ApJS, 138, 185

Fuente, A., Neri, R., Martín-Pintado, J., et al. 2001, A&A, 366, 873

Fuente, A., Neri, R., & Caselli, P. 2005, A&A, 444, 481

Getman, K. V., Feigelson, E. D., Grosso, N., et al. 2005a, ApJS, 160, 353

Getman, K. V., Flaccomio, E., Broos, P. S., et al. 2005b, ApJS, 160, 319

Gutermuth, R. A., Megeath, S. T., Muzerolle, J., et al. 2004, ApJS, 154, 374

Gutermuth, R. A., Myers, P. C., Megeath, S. T., et al. 2008, ApJ, 674, 336

Gutermuth, R. A., Megeath, S. T., Myers, P. C., et al. 2009, ApJS, 184, 18

Haisch, Jr., K. E., Lada, E. A., & Lada, C. J. 2001, ApJ, 553, L153

Hartigan, P., & Lada, C. J. 1985, ApJS, 59, 383

Hartmann, L., Megeath, S. T., Allen, L., et al. 2005, ApJ, 629, 881

Herbig, G. H. 1960, ApJS, 4, 337

Hernández, J., Hartmann, L., Megeath, T., et al. 2007, ApJ, 662, 1067

Hillenbrand, L. A., Strom, S. E., Vrba, F. J., & Keene, J. 1992, ApJ, 397, 613

Indebetouw, R., Mathis, J. S., Babler, B. L., et al. 2005, ApJ, 619, 931

Jørgensen, J. K., Harvey, P. M., Evans, II, N. J., et al. 2006, ApJ, 645, 1246

Kenyon, S. J., & Hartmann, L. 1995, ApJS, 101, 117

Kraft, R. P., Burrows, D. N., & Nousek, J. A. 1991, ApJ, 374, 344

Lada, C. J. 1987, in Star Forming Regions, ed. M. Peimbert, & J. Jugaku, IAU Symp., 115, 1

Lada, C. J., Muench, A. A., Luhman, K. L., et al. 2006, AJ, 131, 1574

Luhman, K. L., Allen, L. E., Allen, P. R., et al. 2008, ApJ, 675, 1375

Magakian, T. Y., Movsessian, T. A., & Nikogossian, E. H. 2004, Astrophys., 47, 519

Marigo, P., Girardi, L., Bressan, A., et al. 2008, A&A, 482, 883

Megeath, S. T., Allen, L. E., Gutermuth, R. A., et al. 2004, ApJS, 154, 367

Meyer, M. R., Calvet, N., & Hillenbrand, L. A. 1997, AJ, 114, 288

Miranda, L. F., Eiroa, C., & Gomez de Castro, A. I. 1993, A&A, 271, 564

Miskolczi, B., Tothill, N. F. H., Mitchell, G. F., & Matthews, H. E. 2001, ApJ, 560, 841

Muzerolle, J., Megeath, S. T., Gutermuth, R. A., et al. 2004, ApJS, 154, 379

Predehl, P., & Schmitt, J. H. M. M. 1995, A&A, 293, 889

Preibisch, T., Kim, Y.-C., Favata, F., et al. 2005, ApJS, 160, 401

Prisinzano, L., Micela, G., Flaccomio, E., et al. 2008, ApJ, 677, 401

Racine, R. 1968, AJ, 73, 233

Raymond, J. C., & Smith, B. W. 1977, ApJS, 35, 419

Reid, I. N., & Gizis, J. E. 1997, AJ, 113, 2246

Reid, I. N., Gizis, J. E., & Hawley, S. L. 2002, AJ, 124, 2721

Rieke, G. H., & Lebofsky, M. J. 1985, ApJ, 288, 618

Robitaille, T. P., Whitney, B. A., Indebetouw, R., & Wood, K. 2007, ApJS, 169, 328

Robitaille, T. P., Whitney, B. A., Indebetouw, R., Wood, K., & Denzmore, P. 2006, ApJS, 167, 256

Schmitt, J. H. M. M., & Liefke, C. 2004, A&A, 417, 651

Shevchenko, V. S., & Yakubov, S. D. 1989, Sov. Astron., 33, 370

Siess, L., Dufour, E., & Forestini, M. 2000, A&A, 358, 593

Stelzer, B., Robrade, J., Schmitt, J. H. M. M., & Bouvier, J. 2009, A&A, 493, 1109

Stern, D., Eisenhardt, P., Gorjian, V., et al. 2005, ApJ, 631, 163

Strom, S. E., Vrba, F. J., & Strom, K. M. 1976, AJ, 81, 638

Strom, K. M., Strom, S. E., Wolff, S. C., Morgan, J., & Wenz, M. 1986, ApJS, 62, 39

Vuong, M. H., Montmerle, T., Grosso, N., et al. 2003, A&A, 408, 581

Watson, A. M., Stapelfeldt, K. R., Wood, K., & Ménard, F. 2007, in Protostars and Planets V, ed. B. Reipurth, D. Jewitt, & K. Keil, 523

Weintraub, D. A., Kastner, J. H., & Mahesh, A. 1994, ApJ, 420, L87

White, R. J., Greene, T. P., Doppmann, G. W., Covey, K. R., & Hillenbrand, L. A. 2007, in Protostars and Planets V, ed. B. Reipurth, D. Jewitt, & K. Keil, 117

Wood, K., Lada, C. J., Bjorkman, J. E., et al. 2002, ApJ, 567, 1183

Table 2. X-ray parameters for all detected sources.

ID	X-ray position		Offax	Expo	Rate	Signif	S/N	$\log L_x{}^a$
	α_{2000}	δ_{2000}	[$'$]	[s]	[10^{-3} cts/s]			[erg/s]
NGC 7129-S3-X1	21 42 59.62	+66 04 33.9	2.4	22462	3.3 ± 0.4	30.0	110.8	30.9
NGC 7129-S3-X2	21 42 47.09	+66 04 57.8	2.8	22193	5.8 ± 0.5	49.4	188.4	30.7
NGC 7129-S3-X3	21 42 46.09	+66 05 13.8	2.7	22224	2.2 ± 0.3	20.1	71.8	30.4
NGC 7129-S3-X4	21 42 34.73	+66 05 18.8	3.7	21969	3.3 ± 0.4	25.5	69.8	30.5
NGC 7129-S3-X6	21 42 58.39	+66 05 27.3	1.7	22587	1.5 ± 0.3	14.9	53.2	30.3
NGC 7129-S3-X7	21 43 18.10	+66 05 35.1	1.6	22499	0.8 ± 0.2	8.5	33.9	30.5
NGC 7129-S3-X8	21 42 49.89	+66 05 42.7	2.1	22397	0.3 ± 0.1	3.2	11.7	29.5
NGC 7129-S3-X9	21 43 16.86	+66 05 48.6	1.4	22516	0.6 ± 0.2	6.4	28.6	30.4
NGC 7129-S3-X10	21 42 56.28	+66 06 02.0	1.4	22548	3.6 ± 0.4	32.9	126.8	30.5
NGC 7129-S3-X11	21 42 50.96	+66 06 03.8	1.9	22489	2.2 ± 0.3	19.4	83.7	30.4
NGC 7129-S3-X12	21 42 58.82	+66 06 10.2	1.1	22595	24.5 ± 1.0	72.4	883.9	...
NGC 7129-S3-X13	21 42 58.60	+66 06 10.3	1.2	22586	25.7 ± 1.1	105.7	942.4	31.4
NGC 7129-S3-X14	21 43 21.07	+66 06 22.8	1.4	22389	1.2 ± 0.2	12.5	58.3	30.1
NGC 7129-S3-X15	21 42 57.22	+66 06 34.8	1.1	22567	0.4 ± 0.1	4.6	15.1	29.6
NGC 7129-S3-X16	21 42 50.19	+66 06 35.0	1.8	22480	3.8 ± 0.4	33.0	136.2	30.6
NGC 7129-S3-X17	21 42 58.77	+66 06 36.8	0.9	22576	1.1 ± 0.2	11.2	45.5	30.2
NGC 7129-S3-X18	21 42 56.77	+66 06 37.2	1.1	22565	1.7 ± 0.3	16.5	62.1	30.7
NGC 7129-S3-X19	21 42 59.99	+66 06 42.5	0.8	22599	0.3 ± 0.1	3.6	15.5	29.6
NGC 7129-S3-X20	21 43 01.89	+66 06 44.7	0.6	21330	2.7 ± 0.4	25.4	99.4	30.5
NGC 7129-S3-X21	21 43 20.90	+66 06 51.8	1.3	22331	0.8 ± 0.2	8.1	37.2	30.2
NGC 7129-S3-X22	21 43 05.01	+66 06 53.2	0.3	22598	2.1 ± 0.3	20.0	83.9	30.4
NGC 7129-S3-X23	21 42 47.92	+66 06 52.9	2.0	22425	5.1 ± 0.5	41.0	197.4	30.7
NGC 7129-S3-X24	21 42 59.78	+66 06 55.7	0.8	22571	1.0 ± 0.2	10.8	37.3	...
NGC 7129-S3-X25	21 42 52.65	+66 06 57.2	1.5	22493	0.8 ± 0.2	7.9	27.7	30.1
NGC 7129-S3-X26	21 42 54.92	+66 07 21.1	1.4	22465	1.2 ± 0.2	11.0	37.7	30.1
NGC 7129-S3-X27	21 43 05.18	+66 07 33.9	0.8	22475	2.0 ± 0.3	19.7	116.4	31.1
NGC 7129-S3-X28	21 43 15.31	+66 07 56.9	1.3	22291	2.8 ± 0.4	27.0	108.6	31.0
NGC 7129-S3-X29	21 42 53.49	+66 08 05.2	1.9	22331	2.8 ± 0.4	24.3	115.6	30.5
NGC 7129-S3-X30	21 43 11.62	+66 09 11.4	2.4	21997	4.0 ± 0.4	34.1	201.6	30.5
NGC 7129-S3-X31	21 42 46.09	+66 05 56.3	2.4	20019	1.2 ± 0.2	11.0	36.6	30.8
NGC 7129-S3-X32	21 42 54.84	+66 06 13.5	1.5	22540	1.0 ± 0.2	6.7	36.4	30.0
NGC 7129-S3-X35	21 42 51.96	+66 06 33.4	1.6	22502	0.5 ± 0.1	4.6	18.0	29.7
NGC 7129-S3-X36	21 42 54.75	+66 06 35.3	1.3	22535	1.2 ± 0.2	12.4	50.0	30.7
NGC 7129-S3-X37	21 42 55.72	+66 06 45.0	1.2	22541	0.2 ± 0.1	3.2	9.7	29.4
NGC 7129-S3-X38	21 43 07.15	+66 06 54.0	0.1	22595	0.7 ± 0.2	6.8	34.9	...
NGC 7129-S3-X39	21 42 46.91	+66 06 57.4	2.1	22383	0.6 ± 0.2	5.7	24.6	29.8
NGC 7129-S3-X40	21 42 45.32	+66 07 04.4	2.3	22327	1.0 ± 0.2	10.6	39.9	30.4
NGC 7129-S3-X41	21 42 38.91	+66 07 08.7	2.9	21036	0.7 ± 0.2	5.0	22.3	...
NGC 7129-S3-X42	21 43 19.39	+66 07 21.4	1.3	22266	0.6 ± 0.2	5.9	26.6	29.8
NGC 7129-S3-X43	21 42 58.34	+66 07 26.3	1.1	21325	0.5 ± 0.2	4.7	17.7	29.7
NGC 7129-S3-X45	21 42 54.08	+66 08 14.9	2.0	21951	0.6 ± 0.2	7.0	22.7	31.2
NGC 7129-S3-X47	21 42 58.26	+66 05 40.0	1.5	22571	0.3 ± 0.1	3.3	10.6	...
NGC 7129-S3-X48	21 42 55.87	+66 05 42.8	1.7	22541	0.4 ± 0.1	3.6	13.4	29.6
NGC 7129-S3-X50	21 43 03.01	+66 06 55.9	0.5	21651	0.4 ± 0.1	4.0	16.3	...
NGC 7129-S3-X51	21 43 01.71	+66 07 08.9	0.7	21646	0.4 ± 0.1	4.6	19.0	29.7
NGC 7129-S3-X52	21 42 40.34	+66 10 07.2	4.3	8466	9.3 ± 1.0	16.7	127.7	31.3
NGC 7129-S3-X53	21 42 24.73	+66 01 41.0	6.8	20570	4.1 ± 0.4	12.5	22.2	31.5
NGC 7129-S3-X56	21 43 29.28	+66 03 31.5	4.0	21103	0.5 ± 0.2	3.9	14.9	29.8
NGC 7129-S3-X58	21 42 19.32	+66 07 26.6	4.9	21272	0.6 ± 0.2	3.7	7.7	...
NGC 7129-S2-X1	21 43 31.80	+66 08 50.5	3.1	22254	1.9 ± 0.3	11.3	104.5	30.7
NGC 7129-S2-X2	21 43 24.89	+66 07 34.1	1.9	10708	1.7 ± 0.4	9.4	68.4	...
NGC 7129-S2-X3	21 43 20.37	+66 08 20.2	2.0	10346	0.8 ± 0.3	4.5	30.3	...
NGC 7129-S2-X4	21 43 27.02	+66 09 36.5	3.4	22154	2.1 ± 0.3	12.7	116.0	30.2
NGC 7129-S2-X5	21 43 43.43	+66 07 30.7	3.7	22071	1.9 ± 0.3	15.7	68.2	30.7
NGC 7129-S2-X7	21 43 53.11	+66 08 09.8	4.8	20210	0.7 ± 0.2	3.9	15.1	...
NGC 7129-S2-X8	21 43 33.96	+66 10 43.4	4.7	19757	1.4 ± 0.3	6.8	37.1	30.5
NGC 7129-S2-X9	21 43 36.29	+66 11 32.9	5.5	19218	5.7 ± 0.5	21.8	99.0	30.8
NGC 7129-S2-X10	21 44 29.55	+66 07 06.8	8.3	19639	1.2 ± 0.3	5.6	17.1	...
NGC 7129-S2-X14	21 44 26.43	+66 10 29.1	8.7	18704	1.0 ± 0.2	4.2	11.0	...

^{a} The X-ray luminosities were computed using the kT and N_H obtained from the hardness ratios as described in Sect. 2. L_x is given only for objects selected as pre-MS candidates with the criteria described in Sect. 5.

Table 3. Identification and offset between X-ray and optical/IR position
for counterparts of X-ray sources.

NGC 7129-...	Name	Δ_{O-X} ['']	Δ_{2M-X} ['']
...-S3-X1	HL85-S 25	0.46	0.10
...-S3-X2		–	0.11
...-S3-X3	HL85-S II	1.82	0.23
...-S3-X4		–	0.22
...-S3-X6		–	0.10
...-S3-X7		–	0.11
...-S3-X8		–	0.11
...-S3-X9	MMN-19	1.15	0.09
...-S3-X10		–	0.10
...-S3-X11		–	0.22
...-S3-X12		–	–
...-S3-X13	SVS 8	1.27	0.07
...-S3-X14		–	1.44
...-S3-X15		–	0.17
...-S3-X16	SVS 7	1.30	0.09
...-S3-X17		–	0.18
...-S3-X18		–	0.10
...-S3-X19		–	0.13
...-S3-X20		–	0.05
...-S3-X21		–	0.08
...-S3-X22		–	0.22
...-S3-X23		–	0.01
...-S3-X24		–	–
...-S3-X25	MMN-6	1.09	0.10
...-S3-X26		–	0.12
...-S3-X27		–	0.17
...-S3-X28		–	0.16
...-S3-X29	MMN-9	1.94	0.18
...-S3-X30	MMN-17	1.30	0.12
...-S3-X31		–	0.13
...-S3-X32	MMN-10	1.94	0.82
...-S3-X35		–	0.27
...-S3-X36	MEG93 Star 2	1.51	0.16
...-S3-X37		–	0.30
...-S3-X38		–	–
...-S3-X39		–	0.13
...-S3-X40		–	0.13
...-S3-X41		–	–
...-S3-X42		–	0.11
...-S3-X43		–	0.09
...-S3-X45		–	0.15
...-S3-X47		–	0.29
...-S3-X48		–	0.29
...-S3-X50		–	–
...-S3-X51	SVS 13	1.49	0.05
...-S3-X52	SVS 2	1.40	0.31
...-S3-X53		–	–
...-S3-X56		–	0.63
...-S3-X58		–	–
...-S2-X1	HL85-N 27	1.42	0.18
...-S2-X2		–	–
...-S2-X3		–	0.54
...-S2-X4		–	0.38
...-S2-X5	MMN-22	1.32	0.14
...-S2-X7		–	–
...-S2-X8		–	–
...-S2-X9	SVS 15	1.96	0.17
...-S2-X10		–	–
...-S2-X14		–	–

Table 4. Photometry and YSO classification for optical and IR counterparts of X-ray sources. Asterisks in column "YSO Class" identify objects selected on basis of near-IR data.

NGC 7129...	V [mag]	R [mag]	I [mag]	J [mag]	H [mag]	K [mag]	[3.6] [mag]	[4.5] [mag]	[5.8] [mag]	[8.0] [mag]	[24] [mag]	YSO Class	AGN?
...S3-X1	18.32	16.23	15.11	12.89 ± 0.03	11.62 ± 0.03	10.95 ± 0.02	10.18 ± 0.00	9.73 ± 0.00	9.39 ± 0.00	8.91 ± 0.02	6.81 ± 0.21	II	
...S3-X2	⋯	⋯	⋯	12.10 ± 0.02	11.33 ± 0.03	11.05 ± 0.02	10.79 ± 0.01	10.74 ± 0.01	10.54 ± 0.09	10.00 ± 0.28	⋯	III	
...S3-X3	10.64	10.39	10.24	10.06 ± 0.02	9.90 ± 0.02	9.83 ± 0.02	9.85 ± 0.00	9.84 ± 0.00	9.87 ± 0.04	9.91 ± 0.16	⋯	III	
...S3-X4	⋯	⋯	⋯	13.92 ± 0.03	13.28 ± 0.04	13.13 ± 0.04	12.87 ± 0.01	12.80 ± 0.01	12.82 ± 0.05	13.06 ± 0.19	⋯	III	
...S3-X5	⋯	⋯	⋯	13.96 ± 0.03	13.03 ± 0.03	12.64 ± 0.03	11.79 ± 0.03	11.39 ± 0.03	⋯	⋯	⋯	II*	
...S3-X6	⋯	⋯	⋯	13.99 ± 0.03	13.70 ± 0.05	13.39 ± 0.01	13.27 ± 0.01	13.29 ± 0.17	13.12 ± 0.28	⋯	⋯	II*	
...S3-X7	⋯	⋯	⋯	14.76 ± 0.04	13.72 ± 0.06	13.53 ± 0.03	13.39 ± 0.04	13.27 ± 0.07	13.05 ± 0.11	⋯	⋯	II	
...S3-X8	⋯	⋯	⋯	14.65 ± 0.05	14.01 ± 0.06	13.72 ± 0.06	13.39 ± 0.03	13.27 ± 0.03	⋯	⋯	⋯	III	
...S3-X9	18.42	17.12	⋯	14.18 ± 0.03	13.30 ± 0.04	12.74 ± 0.01	12.57 ± 0.01	12.45 ± 0.09	11.99 ± 0.12	⋯	6.50 ± 0.21	III	
...S3-X10	⋯	16.00	⋯	13.66 ± 0.03	13.12 ± 0.04	12.57 ± 0.01	11.41 ± 0.03	11.13 ± 0.09	10.78 ± 0.39	⋯	⋯	III	
...S3-X11	⋯	⋯	⋯	13.64 ± 0.03	12.80 ± 0.04	12.55 ± 0.03	12.42 ± 0.03	12.37 ± 0.03	12.24 ± 0.43	⋯	⋯	III	
...S3-X12	⋯	⋯	⋯	⋯	⋯	⋯	⋯	⋯	⋯	⋯	⋯	III	
...S3-X13	⋯	⋯	⋯	8.98 ± 0.02	8.66 ± 0.02	8.51 ± 0.02	8.48 ± 0.02	8.48 ± 0.03	8.42 ± 0.09	8.00 ± 0.28	⋯	III	
...S3-X14	⋯	⋯	⋯	13.56 ± 0.03	12.90 ± 0.04	12.75 ± 0.04	12.44 ± 0.00	12.44 ± 0.00	12.32 ± 0.03	12.42 ± 0.10	⋯	III	
...S3-X15	⋯	⋯	⋯	13.67 ± 0.05	12.75 ± 0.05	12.53 ± 0.03	12.53 ± 0.03	12.00 ± 0.04	⋯	⋯	⋯	II	
...S3-X16	⋯	⋯	⋯	8.97 ± 0.02	8.73 ± 0.02	8.47 ± 0.02	8.13 ± 0.00	7.90 ± 0.00	7.57 ± 0.01	7.09 ± 0.05	⋯	III	
...S3-X17	⋯	⋯	⋯	13.49 ± 0.03	12.56 ± 0.03	12.34 ± 0.03	11.98 ± 0.03	11.85 ± 0.04	10.44 ± 0.26	⋯	⋯	II*	
...S3-X18	⋯	⋯	⋯	12.56 ± 0.03	12.34 ± 0.03	11.47 ± 0.05	11.21 ± 0.04	11.15 ± 0.04	⋯	⋯	⋯	II*	
...S3-X19	⋯	⋯	⋯	14.35 ± 0.05	13.49 ± 0.04	13.15 ± 0.04	13.05 ± 0.07	13.05 ± 0.11	⋯	⋯	⋯	II	
...S3-X20	⋯	⋯	⋯	13.30 ± 0.03	12.69 ± 0.03	12.73 ± 0.04	12.21 ± 0.03	11.78 ± 0.00	⋯	⋯	⋯	II	
...S3-X21	⋯	⋯	⋯	15.52 ± 0.07	13.79 ± 0.05	11.12 ± 0.03	10.80 ± 0.01	10.80 ± 0.02	11.15 ± 0.41	12.30 ± 0.05	⋯	II*	
...S3-X22	⋯	⋯	⋯	13.05 ± 0.04	12.02 ± 0.04	12.54 ± 0.03	12.40 ± 0.01	12.40 ± 0.01	12.24 ± 0.02	⋯	⋯	III	
...S3-X23	⋯	⋯	⋯	13.46 ± 0.03	12.42 ± 0.03	12.09 ± 0.03	11.26 ± 0.07	11.71 ± 0.01	10.89 ± 0.12	⋯	⋯	III	
...S3-X24	⋯	⋯	⋯	⋯	⋯	⋯	11.69 ± 0.02	11.71 ± 0.01	10.89 ± 0.12	⋯	⋯	III	
...S3-X25	18.30	17.04	15.78	13.82 ± 0.03	12.65 ± 0.03	12.50 ± 0.03	10.24 ± 0.00	9.77 ± 0.04	9.77 ± 0.04	9.15 ± 0.06	⋯	II	
...S3-X26	⋯	⋯	⋯	14.25 ± 0.05	13.19 ± 0.06	12.84 ± 0.04	12.50 ± 0.03	12.44 ± 0.03	11.96 ± 0.28	⋯	⋯	III	
...S3-X27	⋯	⋯	>17.89	15.01 ± 0.05	>15.97	13.03 ± 0.01	13.03 ± 0.01	12.69 ± 0.01	12.41 ± 0.25	11.28 ± 0.44	⋯	II	
...S3-X28	⋯	⋯	⋯	13.34 ± 0.04	12.59 ± 0.03	11.57 ± 0.01	11.03 ± 0.01	10.41 ± 0.01	10.41 ± 0.01	9.41 ± 0.01	4.98 ± 0.02	II	
...S3-X29	17.66	16.22	14.97	13.21 ± 0.03	12.36 ± 0.03	11.78 ± 0.02	11.85 ± 0.01	11.22 ± 0.08	11.22 ± 0.08	⋯	⋯	II	
...S3-X30	16.31	15.23	14.14	12.60 ± 0.02	11.80 ± 0.03	11.04 ± 0.00	10.73 ± 0.00	10.38 ± 0.01	10.38 ± 0.01	9.70 ± 0.01	7.63 ± 0.05	II	
...S3-X31	⋯	16.19	⋯	13.79 ± 0.03	13.02 ± 0.03	12.58 ± 0.01	12.60 ± 0.01	12.57 ± 0.09	12.57 ± 0.09	13.15 ± 0.90	⋯	III	
...S3-X32	17.78	17.51	16.19	14.19 ± 0.03	13.25 ± 0.03	12.91 ± 0.04	12.75 ± 0.03	12.58 ± 0.01	⋯	⋯	⋯	III	
...S3-X35	⋯	⋯	⋯	14.04 ± 0.04	13.31 ± 0.04	12.63 ± 0.04	12.58 ± 0.05	12.68 ± 0.02	⋯	⋯	⋯	III	
...S3-X36	⋯	⋯	⋯	14.18 ± 0.05	13.18 ± 0.06	12.56 ± 0.04	11.66 ± 0.02	11.37 ± 0.02	11.02 ± 0.19	10.05 ± 0.39	⋯	II	
...S3-X37	⋯	⋯	15.58 ± 0.08	14.58 ± 0.06	14.27 ± 0.08	13.62 ± 0.07	13.37 ± 0.06	⋯	⋯	⋯	⋯	III	
...S3-X38	⋯	⋯	13.60 ± 0.04	13.98 ± 0.05	13.39 ± 0.05	13.13 ± 0.05	13.05 ± 0.05	13.05 ± 0.05	⋯	⋯	⋯	III	
...S3-X39	⋯	⋯	14.99 ± 0.05	>12.40	13.13 ± 0.05	11.24 ± 0.01	10.91 ± 0.01	10.55 ± 0.09	10.55 ± 0.09	9.74 ± 0.22	⋯	II	
...S3-X40	⋯	⋯	⋯	>12.40	>11.97	11.24 ± 0.01	10.91 ± 0.01	10.55 ± 0.01	⋯	⋯	⋯	III	
...S3-X41	⋯	⋯	15.06 ± 0.05	14.29 ± 0.07	13.89 ± 0.08	13.90 ± 0.05	13.72 ± 0.05	13.62 ± 0.06	13.43 ± 0.16	13.43 ± 0.16	⋯	III	
...S3-X42	⋯	⋯	14.31 ± 0.03	12.62 ± 0.03	11.91 ± 0.03	11.44 ± 0.03	11.39 ± 0.03	10.93 ± 0.44	10.93 ± 0.44	⋯	⋯	II	
...S3-X43	⋯	⋯	14.42 ± 0.04	13.25 ± 0.04	12.82 ± 0.04	12.52 ± 0.01	12.55 ± 0.01	12.29 ± 0.21	11.25 ± 0.50	11.25 ± 0.50	⋯	II	
...S3-X45	⋯	⋯	⋯	⋯	⋯	⋯	⋯	⋯	⋯	⋯	⋯	⋯	
...S3-X47	⋯	⋯	>14.17	>13.38	>13.38	⋯	⋯	⋯	⋯	⋯	⋯	III	
...S3-X48	⋯	⋯	15.21 ± 0.06	14.37 ± 0.07	13.97 ± 0.09	13.43 ± 0.27	13.38 ± 0.38	13.38 ± 0.38	⋯	⋯	⋯	III	
...S3-X50	⋯	⋯	⋯	⋯	⋯	12.79 ± 0.21	12.59 ± 0.20	⋯	⋯	⋯	⋯	⋯	

Table 4. Continued.

Name													
...-S3-X51	...	...	...	11.24 ± 0.04	10.56 ± 0.04	>10.25	9.19 ± 0.07	8.81 ± 0.05	...	...	...	III	
...-S3-X52	...	...	...	11.00 ± 0.02	10.71 ± 0.03	10.58 ± 0.02	10.52 ± 0.00	10.52 ± 0.00	10.27 ± 0.02	9.73 ± 0.07	...	II	
...-S3-X53	...	...	...	...	...	...	14.88 ± 0.02	14.22 ± 0.02	13.43 ± 0.05	12.62 ± 0.05	...	II	
...-S3-X56	...	...	...	10.02 ± 0.02	9.73 ± 0.03	9.69 ± 0.02	9.69 ± 0.00	9.69 ± 0.00	9.64 ± 0.00	9.64 ± 0.01	8.41 ± 0.07	III	V
...-S3-X58	...	...	...	...	...	...	...	...	...	...	10.09 ± 0.18	III	
...-S2-X1	18.12	17.04	15.82	13. ± 0.03	12.89 ± 0.03	12.30 ± 0.03	11.59 ± 0.00	11.29 ± 0.00	11.02 ± 0.01	10.31 ± 0.01	7.35 ± 0.05	II	
...-S2-X2	...	...	...	...	...	...	17.12 ± 0.23	16.15 ± 0.12	...	...	...	...	
...-S2-X3	...	...	...	>16.66	14.76 ± 0.08	13.60 ± 0.05	12.81 ± 0.01	12.60 ± 0.01	12.46 ± 0.02	12.32 ± 0.06	...	III	
...-S2-X4	...	...	...	13.61 ± 0.03	12.90 ± 0.03	12.72 ± 0.03	12.67 ± 0.00	12.66 ± 0.01	12.60 ± 0.02	12.55 ± 0.05	...	III	
...-S2-X5	18.25	16.82	15.56	13.65 ± 0.03	12.61 ± 0.03	12.15 ± 0.03	11.43 ± 0.00	11.05 ± 0.00	10.63 ± 0.01	10.06 ± 0.01	7.83 ± 0.05	II	V
...-S2-X7	...	...	...	...	...	...	...	...	...	...	...	...	
...-S2-X8	...	...	...	...	...	...	16.53 ± 0.06	15.46 ± 0.04	14.34 ± 0.11	13.33 ± 0.10	...	0/I	
...-S2-X9	...	...	...	11.77 ± 0.02	11.29 ± 0.03	11.17 ± 0.02	11.13 ± 0.00	11.11 ± 0.00	11.07 ± 0.01	11.06 ± 0.	...	III	
...-S2-X10	...	...	...	...	...	...	...	...	...	...	...	...	
...-S2-X14	...	...	...	...	...	...	...	...	...	...	...	...	

Table 5. X-ray upper limits and 2 MASS counterparts for Class I sources not detected in X-rays.

ID	2 MASS position		Offax	Expo	Rate	$\log L_x$
	α_{2000}	δ_{2000}	[']	[s]	$[10^{-3}$ cts/s]	[erg/s]
NGC 7129-S3-U419	21 43 01.78	+66 03 24.4	3.5	21 865	<0.2	<29.7
NGC 7129-S3-U546	21 42 57.75	+66 04 23.5	2.7	22 270	<0.3	<29.8
NGC 7129-S3-U968	21 43 06.96	+66 06 41.7	0.2	22 640	<0.1	<29.5
NGC 7129-S3-U1059	21 43 24.90	+66 07 04.7	1.7	11 355	<0.3	<29.8
NGC 7129-S3-U1169	21 43 14.83	+66 07 37.5	1.0	22 349	<0.2	<29.7
NGC 7129-S3-U1178	21 41 55.30	+66 07 41.5	7.4	10 077	<1.4	<30.5
NGC 7129-S3-U1211	21 43 14.17	+66 07 46.5	1.1	22 328	<0.2	<29.7
NGC 7129-S3-U1242	21 43 05.92	+66 07 58.5	1.1	22 367	<0.1	<29.5
NGC 7129-S3-U1521	21 42 42.86	+66 09 24.0	3.6	21 139	<0.2	<29.7
NGC 7129-S2-U1350	21 43 24.13	+66 08 31.5	2.3	22 573	<0.3	<29.8
NGC 7129-S3-U270	21 42 59.82	+66 01 54.9	5.0	20 825	<0.1	<29.5
NGC 7129-S3-U500	21 43 02.01	+66 04 02.7	2.9	22 274	<0.1	<29.5
NGC 7129-S3-U550	21 43 11.17	+66 04 25.6	2.5	22 485	<0.2	<29.7
NGC 7129-S3-U722	21 42 54.63	+66 05 20.3	2.0	22 520	<0.3	<29.8
NGC 7129-S3-U815	21 42 51.43	+66 05 56.4	1.9	22 499	<0.2	<29.7
NGC 7129-S3-U821	21 43 29.32	+66 05 55.7	2.4	20 607	<0.2	<29.5
NGC 7129-S3-U822	21 43 04.38	+66 05 56.4	1.0	22 647	<0.1	<29.5
NGC 7129-S3-U840	21 42 23.08	+66 06 04.5	4.6	21 643	<0.6	<30.1
NGC 7129-S3-U849	21 43 12.30	+66 06 05.6	0.9	22 600	<0.3	<29.8
NGC 7129-S3-U939	21 42 38.81	+66 06 36.0	2.9	22 113	<0.2	<29.7
NGC 7129-S3-U1012	21 43 06.81	+66 06 54.3	0.1	22 600	<0.6	<30.1
NGC 7129-S3-U1026	21 43 12.42	+66 06 55.9	0.5	22 507	<0.2	<29.7
NGC 7129-S3-U1085	21 42 53.13	+66 07 14.8	1.5	22 465	<0.3	<29.8
NGC 7129-S3-U1103	21 43 07.84	+66 07 18.5	0.5	22 477	<0.1	<29.5
NGC 7129-S3-U1107	21 42 55.92	+66 07 20.9	1.3	22 470	<0.5	<30.1
NGC 7129-S3-U1109	21 42 53.21	+66 07 20.9	1.6	22 454	<0.5	<30.1
NGC 7129-S3-U1194	21 42 42.42	+66 07 45.2	2.7	22 107	<0.2	<29.7
NGC 7129-S3-U1246	21 42 48.23	+66 08 00.6	2.3	22 214	<0.4	<30.0
NGC 7129-S3-U1294	21 43 02.89	+66 08 14.2	1.5	22 316	<0.1	<29.5
NGC 7129-S3-U1367	21 42 17.67	+66 08 40.3	5.4	19 816	<0.5	<30.0
NGC 7129-S3-U1433	21 43 14.40	+66 08 58.7	2.2	15 537	<0.2	<29.7
NGC 7129-S3-U1504	21 42 53.47	+66 09 19.7	2.9	21 725	<0.2	<29.7
NGC 7129-S3-U1522	21 42 41.92	+66 09 24.5	3.7	21 067	<0.1	<29.5
NGC 7129-S3-U1542	21 43 05.17	+66 09 29.4	2.6	21 816	<0.1	<29.5
NGC 7129-S3-U1611	21 43 02.62	+66 09 50.7	3.0	21 560	<0.3	<29.8
NGC 7129-S3-U1612	21 42 40.55	+66 09 51.8	4.1	20 281	<0.5	<30.0
NGC 7129-S3-U1780	21 42 59.47	+66 10 35.8	3.8	20 598	<0.3	<29.9
NGC 7129-S2-U613	21 43 48.70	+66 04 46.2	4.6	21 164	<0.2	<29.7
NGC 7129-S2-U804	21 43 33.12	+66 05 49.0	2.8	9668	<0.3	<29.9
NGC 7129-S2-U820	21 44 05.38	+66 05 53.3	5.9	19 261	<0.6	<30.1
NGC 7129-S2-U1083	21 43 29.92	+66 07 09.2	2.3	20 393	<0.2	<29.7
NGC 7129-S2-U1313	21 43 26.64	+66 08 20.5	2.4	22 559	<0.1	<29.5
NGC 7129-S2-U1640	21 43 12.35	+66 09 55.5	3.1	10 420	<0.3	<29.8
NGC 7129-S2-U1660	21 43 47.04	+66 10 01.2	5.1	21 507	<0.4	<29.9
NGC 7129-S2-U1713	21 43 49.35	+66 10 12.9	5.4	17 909	<0.4	<29.9
NGC 7129-S2-U2219	21 43 38.59	+66 12 30.6	6.5	14 592	<0.6	<30.1

[a] The upper limits to the X-ray luminosity were computed using the median of kT and N_H from the sample of X-ray detected Class II sources. These numbers may be underestimated if the extinction is much higher, as is expected for the Class I sources (see Sect. 6.4).

Table 6. Candidate YSOs without X-ray emission selected on basis of their IR photometry. Asterisks in column "YSO Class" identify objects selected on basis of near-IR data.

NGC 7129-...	Name	Δ_{O-S} ['']	V [mag]	R [mag]	I [mag]	J [mag]	H [mag]	K [mag]	[3.6] [mag]	[4.5] [mag]	[5.8] [mag]	[8.0] [mag]	[24] [mag]	YSO Class	AGN?
…S3-U419		—	…	…	…	…	13.66±0.07	13.02±0.02	10.41±0.01	10.17±0.01	9.08±0.01	…	…	I	
…S3-U546		—	…	…	…	13.23±0.06	10.89±0.03	7.54±0.01	6.59±0.00	5.67±0.00	5.06±0.02	5.06±0.01	5.18±0.05	I	
…S3-U968		—	…	…	…	…	…	…	…	…	…	…	…	I	
…S3-U1059		—	…	…	…	…	14.23±0.01	14.23±0.01	13.33±0.01	12.59±0.02	11.56±0.02	10.22±0.05	5.34±0.03	I	
…S3-U1169		—	…	…	…	…	14.77±0.14	12.93±0.04	10.72±0.02	10.44±0.02	10.22±0.05	…	4.51±0.07	I	
…S3-U1178		—	…	…	…	…	…	15.86±0.05	14.90±0.03	13.98±0.08	12.78±0.05	…	9.49±0.15	I	
…S3-U1211		—	…	…	…	17.48±0.37	14.34±0.10	10.55±0.00	9.34±0.00	8.41±0.00	7.51±0.00	7.51±0.00	3.55±0.03	I	
…S3-U1242		—	…	…	…	…	…	12.70±0.01	12.70±0.01	12.10±0.06	11.65±0.11	11.65±0.11	…	I	
…S3-U1521		—	…	…	…	…	…	13.78±0.01	13.84±0.09	13.84±0.09	12.79±0.17	12.79±0.17	…	I	
…S2-U1350		—	…	…	…	…	12.86±0.01	11.28±0.01	10.05±0.01	8.96±0.01	8.96±0.01	8.96±0.01	4.32±0.00	I	✓
…S3-U270		—	…	…	…	…	…	16.83±0.06	16.59±0.08	15.91±0.26	14.33±0.14	14.33±0.14	…	II	
…S3-U500		—	…	…	…	…	…	13.64±0.01	12.98±0.01	12.18±0.04	11.29±0.07	11.29±0.07	…	II	
…S3-U550		—	…	…	…	…	…	13.91±0.01	13.42±0.01	12.98±0.08	12.33±0.18	12.33±0.18	…	II*	
…S3-U722	MMN-5	1.72	20.35	18.77	17.28	15.52±0.08	14.56±0.08	13.87±0.08	12.51±0.14	12.64±0.14	…	…	8.95±0.15	II*	
…S3-U815		—	…	…	…	14.48±0.10	13.57±0.06	12.62±0.04	12.51±0.01	12.48±0.18	11.78±0.26	…	…	II*	
…S3-U821		—	…	…	…	14.13±0.06	13.39±0.07	13.91±0.01	13.04±0.01	13.05±0.02	12.48±0.18	…	…	II	
…S3-U822		—	…	…	…	15.88±0.10	14.47±0.12	13.47±0.01	13.04±0.01	13.04±0.01	12.98±0.08	…	…	II	
…S3-U840	MMN-1	1.42	20.11	19.02	17.52	15.70±0.10	14.39±0.10	13.39±0.02	13.05±0.02	12.52±0.02	…	…	…	II*	
…S3-U849	HL85-S 14	1.79	18.67	17.66	16.45	15.06±0.05	14.05±0.05	10.59±0.00	10.59±0.00	10.42±0.04	10.19±0.16	11.02±0.14	8.95±0.15	II*	
…S3-U939	SVS 12	1.83	…	…	…	14.80±0.05	13.48±0.04	5.79±0.00	5.15±0.00	4.45±0.00	3.33±0.03	3.33±0.03	…	II*	
…S3-U1012		—	…	…	…	9.53±0.02	8.20±0.02	7.08±0.00	5.79±0.00	5.15±0.00	…	…	…	II	
…S3-U1026		—	…	…	…	15.06±0.05	13.94±0.07	14.16±0.01	14.16±0.01	13.25±0.07	12.23±0.	12.23±0.	…	II	
…S3-U1085	MMN-7	1.33	20.58	19.66	18.24	14.85±0.09	14.16±0.07	14.15±0.01	13.73±0.07	13.25±0.27	9.57±0.11	9.57±0.11	…	II	
…S3-U1103		—	…	…	…	14.60±0.04	13.04±0.06	10.93±0.01	10.93±0.01	11.76±0.21	10.88±0.40	10.88±0.40	…	II	
…S3-U1107		—	…	…	…	14.34±0.04	12.47±0.03	10.54±0.01	10.54±0.01	9.98±0.08	9.02±0.17	9.02±0.17	…	II	
…S3-U1109		—	…	…	…	13.19±0.05	12.68±0.05	11.29±0.01	11.29±0.01	10.82±0.12	9.92±0.29	9.92±0.29	…	II	
…S3-U1194		—	…	…	…	14.23±0.05	13.45±0.05	12.56±0.02	12.21±0.01	12.23±0.18	11.68±0.56	11.68±0.56	…	II	
…S3-U1246		—	…	…	…	13.89±0.04	13.08±0.04	11.69±0.01	11.14±0.00	10.62±0.03	9.67±0.06	9.67±0.06	…	II	
…S3-U1294		—	…	…	…	16.34±0.14	14.15±0.01	14.15±0.01	13.83±0.01	13.58±0.12	12.43±0.48	12.43±0.48	9.29±0.13	II*	
…S3-U1367		—	…	…	…	16.17±0.12	14.63±0.10	13.68±0.01	13.83±0.01	12.91±0.04	12.40±0.04	12.40±0.04	…	II	
…S3-U1433		—	…	…	…	15.02±0.11	14.93±0.16	14.23±0.01	13.23±0.01	13.59±0.04	12.98±0.05	12.98±0.05	…	II	
…S3-U1504	MMN-8	1.57	21.06	19.99	19.01	15.30±0.12	14.58±0.12	12.91±0.01	13.89±0.01	11.87±0.02	11.23±0.04	11.23±0.04	8.47±0.20	II	
…S3-U1522		21.06	…	…	…	15.50±0.14	13.99±0.07	13.56±0.01	12.36±0.01	13.08±0.04	12.30±0.11	12.30±0.11	…	II	
…S3-U1542		—	…	…	…	15.18±0.05	14.34±0.06	14.23±0.01	14.07±0.01	13.70±0.04	13.11±0.07	13.11±0.07	…	II	
…S3-U1611		—	…	…	…	15.16±0.12	14.90±0.15	13.54±0.01	13.16±0.01	12.65±0.02	11.93±0.03	11.93±0.03	…	II	
…S3-U1612		—	…	…	…	15.79±0.09	14.20±0.09	13.54±0.01	13.12±0.01	12.33±0.01	10.48±0.	10.48±0.	8.86±0.12	II	
…S3-U1780		—	…	…	…	15.71±0.09	14.79±0.08	13.12±0.01	13.00±0.01	11.54±0.02	12.05±0.04	12.05±0.04	6.01±0.07	II	
…S2-U613		—	…	…	…	16.05±0.23	14.61±0.12	13.54±0.01	13.54±0.01	12.52±0.02	10.87±0.01	10.87±0.01	7.57±0.03	II	
…S2-U804		—	…	…	14.88±0.05	13.65±0.05	13.08±0.04	12.40±0.00	12.15±0.00	11.83±0.01	13.37±0.07	13.37±0.07	9.14±0.11	II	✓
…S2-U820		—	…	…	13.69±0.03	12.15±0.03	11.22±0.03	9.83±0.00	9.33±0.00	8.92±0.00	8.16±0.00	8.16±0.00	4.72±0.00	II	✓
…S2-U1083		—	…	…	…	14.81±0.04	14.67±0.01	14.19±0.02	14.24±0.02	13.99±0.08	13.38±0.08	13.38±0.08	…	II	
…S2-U1313		—	…	…	…	13.90±0.05	13.59±0.05	14.66±0.02	14.19±0.02	13.79±0.05	13.24±0.06	13.24±0.06	…	II	✓
…S2-U1640		—	…	…	…	14.70±0.09	14.19±0.09	13.00±0.01	12.74±0.01	12.39±0.02	11.85±0.03	11.85±0.03	9.43±0.17	II	
…S2-U1660		—	…	…	…	15.07±0.11	14.05±0.02	14.05±0.01	14.05±0.01	13.72±0.09	13.00±0.17	13.00±0.17	…	II	✓
…S2-U1713		—	…	…	…	15.86±0.10	14.86±0.15	14.53±0.01	14.47±0.02	14.29±0.13	13.36±0.22	13.36±0.22	…	II	
…S2-U2219		—	…	…	…	14.59±0.09	…	13.58±0.01	13.34±0.01	12.80±0.04	11.99±0.05	11.99±0.05	9.47±0.14	II	